buildings

MDPI

Article

Effect of High-Rise Residential Building Layout on the Spatial Vertical Wind Environment in Harbin, China

Ming Lu [1,2], Di Song [1,2,*], Da Shi [1,2], Jing Liu [1,2] and Lu Wang [1,2]

[1] School of Architecture, Harbin Institute of Technology, 66 Xidazhi Street, Harbin 150006, China; hitlm@126.com (M.L.); rongxi139@163.com (D.S.); liujinghit0@163.com (J.L.); wanglu_annie@163.com (L.W.)
[2] Key Laboratory of Cold Region Urban and Rural Human Settlement Environment Science and Technology, Ministry of Industry and Information Technology, 66 Xidazhi Street, Harbin 150006, China
* Correspondence: 18b934024@stu.hit.edu.cn

Abstract: Reasonable building height distribution in urban residential areas is conducive to smoother vertical airflow exchange and promotes sustainable development. This paper studies the influence of building layouts on vertical ventilation in high-rise residential areas in Harbin, China, and discusses typical building layout objectives. The ideal area of 220 × 220 m was determined using statistical analysis and specification requirements, and seven typical layouts were defined based on the distribution of building heights. The computation fluid dynamics (CFD) simulation was verified using wind tunnel testing to improve the accuracy of the Phoenics simulation software. Wind speed, wind pressure, and the Universal Thermal Climate Index (UTCI) in residential areas distributed at different heights were analyzed and evaluated. The results indicated that the Phoenics simulation parameter settings, verified via wind tunnel testing, could achieve reasonable simulation results and different height distribution modes had an impact on the changes in wind speed and wind pressure. The equal-height layout that conformed to the row spacing of the buildings and the layout of taller buildings on the east side could provide higher comfort, and did not require enclosed and downwind layouts. This research can inform the green and livable design of residential buildings and provide a new perspective for the construction of high-rise residential areas in cold cities.

Keywords: computational fluid dynamics; vertical wind environment; space comfort; urban high-rise residential area; height distribution model

Citation: Lu, M.; Song, D.; Shi, D.; Liu, J.; Wang, L. Effect of High-Rise Residential Building Layout on the Spatial Vertical Wind Environment in Harbin, China. *Buildings* **2022**, *12*, 705. https://doi.org/10.3390/buildings12060705

Academic Editor: Ambrose Dodoo

Received: 26 April 2022
Accepted: 21 May 2022
Published: 24 May 2022

1. Introduction

With China's rapid urbanization [1], the urban canopy is increasing, with the increase in high-rise buildings having a more prominent impact on the urban wind environment [2,3]. The footprint of urban residential areas is the largest both on a spatial and population scale. The impact of wind on daily life in this area mainly relates to comfort [4], safety [5,6], and cleanliness [7]. A suitable wind environment can accelerate the evaporation of moisture, thereby reducing the temperature and humidity on the skin, thus increasing comfort. Wind that exceeds a certain velocity picks up debris and hinders outdoor activities, including unbalancing pedestrians, which can result in falls and injuries. Moreover, an appropriate wind environment can accelerate the diffusion of pathogens and pollutants in the air [8]. Under the premise that COVID-19 will persist, ensuring clean air in the residential canopy area will be beneficial to human health [9]. The focus of this study was predominantly on pedestrian elevation, and the evaluation and improvement relating to the wind environment was carried out on the vertical plane range [10,11].

Presently, field measurements, wind tunnel tests, and numerical simulations are being used in other research to study the wind environment. Large amounts of urban spatial data can be obtained by measuring air velocity in the field, however the boundary conditions and parameters cannot be controlled, the influencing factors are complex, and the data are difficult to reproduce, leading to a weak universality of influence. Wind tunnel testing is one

of the main simulation methods used in fluid mechanics [12] and widely used for building layout, wind pressure distribution calculation, and computational fluid dynamics (CFD) simulation verification [13,14]. However, wind tunnel tests do pose certain limitations, such as increased costs, lengthy preparation time, and cumbersome model building. Moreover, it is difficult to meet all the physical parameters involved in a single experiment because the model often needs to be scaled down due to the size of the coverage area. In comparison, numerical simulation has lower costs, controllable boundary conditions, higher accuracy, and improved visibility. With the improvement in computer performance, the accuracy of reproducing results is improved, with the method therefore being widely used [15,16].

CFD usage has become mainstream with an increasing number of architectural designers and planners making use of it to optimize designs to limit the effects of the wind environment and increase natural ventilation, thus improving human comfort [17]. In recent years, CFD simulation has provided an important tool for urban design schemes and policy making, and has been widely used in model development, case studies, and spatial adaptation measures [18]. Jin et al. performed a CFD simulation of wind environments in 24 typical residential areas in cold regions of China and based on the average pedestrian height air velocity ratio, obtained the influence rule for high-rise building locations in multi-elevation mixed residential areas [19]. Li et al. used CFD simulation and other means to analyze the effect of air velocity and building layout on pollutant diffusion in residential areas and to assess the connectivity between trunk roads and residential areas [20]. Antoniou et al. used CFD to simulate and analyze air velocity in the city center and new urban districts [21]. Zeng used CFD simulation based on climate data from the city of Tianjin, China, to analyze air velocity and wind pressure by considering different residential building layout scenarios. The simulation identified the most suitable layout and windproof measures for residential buildings in cold regions [22]. Wang used CFD simulation to analyze three typical mixed residential areas in Hefei city, China, and recommended suitable building heights and planning layouts [23]. Huang et al. selected air velocity, wind pressure, air velocity ratio, and other parameters to conduct comparative analyses on the effect of typical building layout models on ventilation in Hefei, China [24].

The research has shown that the urban wind environment is influenced by different building heights and therefore has a significant impact on comfort levels at varying locations. Previous studies have used wind tunnel testing and numerical modeling to explore the relationship between changes in building design and layouts and wind fields in urban residential areas. It is evident that the research to date on the wind environment in residential areas has focused on the comfort level relating to pedestrian height. Even with differences in building heights, the purpose of studies was to focus on the influence of building height change on the pedestrian height wind environment. With the increase in high-rise buildings, people's spatial position is becoming more elevated. Additionally, with respect to indoor and outdoor air exchange, the comfort needs of people are also affected at pedestrian height. It is therefore necessary to conduct research on the change and quality of the wind environment in a vertical direction.

In summary, the main purposes of this study are listed below.

(1) Whereas previous wind environment research has focused on the effect of pedestrian heights, this study has focused on analyzing the wind environment on the vertical plane and to clarify the factors influencing its variation.
(2) To increase the reliability of the data by combining wind tunnel testing and numerical simulation, to research and select the method of stratified sampling to construct typical non-uniform layout conditions in Harbin, and to conduct simultaneous wind environment simulations to verify the CFD model. The accurate Phoenics CFD program, after meeting the required standard, performed the simulation and extracted data from high-rise residential areas.
(3) With reference to previous studies on urban residential areas, air velocity, wind pressure, wind pressure difference, and Universal Thermal Climate Index (UTCI) were selected as parameters to describe the wind environment. The variation law

of the wind environment on the vertical plane and the effect on comfort levels were evaluated. Because it identifies a suitable layout for construction developments, it can provide reference for the future spatial planning and construction of residential areas in cold regions.

This paper is presented as follows: Section 2 provides details of the research subject and the working methods of numerical simulation and wind tunnel verification. Section 3 compares the wind tunnel testing and numerical simulation results and the data are analyzed. Section 4 draws conclusions and suggestions based on the analysis of the data.

2. Materials and Methods

2.1. High-Rise Residential Area Data

The data for this study was mainly derived from the residential building data (2019) in Harbin's major built-up areas, which recorded 32,495 residential buildings, obtained from the Baidu Map database and verified by field observation. Major built-up areas in Harbin were screened based on the criteria for high-rise buildings defined in accordance with the National Unified Standard for Civil Building Design (GB50352-2019) and the Code for Fire Protection of Building Design (GB50016-2014) [25,26]. In addition, in accordance with the relevant provisions of the Residential Design Code (GB50096-2011) and the Urban Residential Planning and Design Standard (GB50180-2018) [27,28], the high-rise residential area in this study refers to the residential area with a building height exceeding 10 floors (greater than 30 m). As indicated in Figure 1, there are 5918 buildings in total.

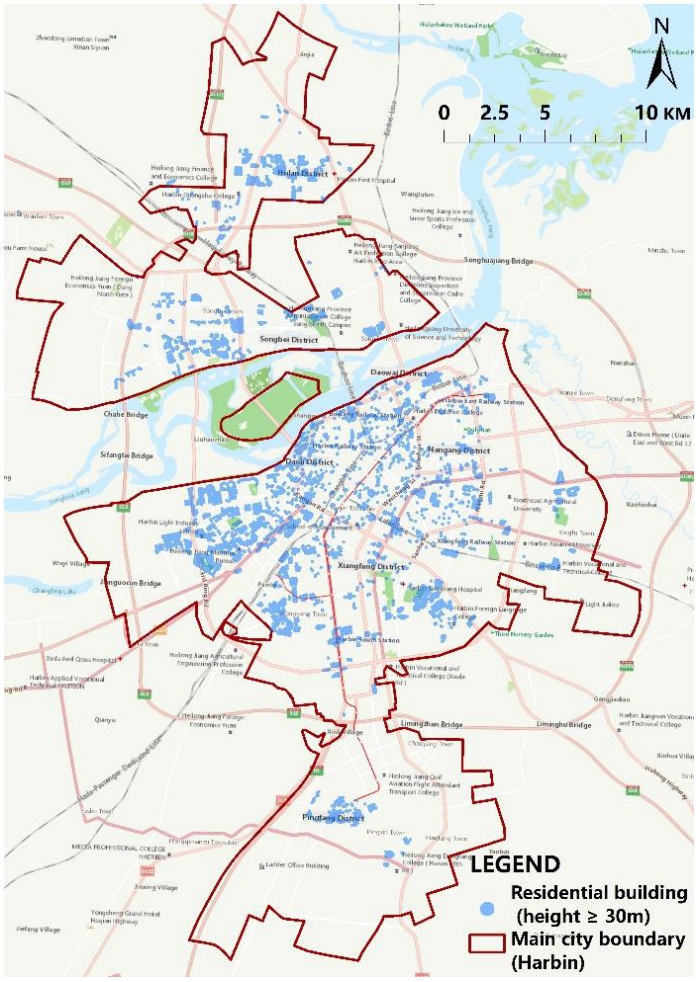

Figure 1. Harbin high-rise residential building layout map.

Moreover, the field survey found that high-rise residential buildings in Harbin were distributed in 126 residential areas, each with at least two or more such buildings. The distribution was generally scattered, but in new areas of the city high-rise residential buildings were more widely distributed. The average floor area was 8.2 ha, as shown in Figure 2a, and most high-rise residential complexes covered 0–5 ha. The number of residential areas with between five and 10 buildings was 49. Residential high-rise buildings under construction had to be redesigned because the change in the city's laws led to a change of monomer architecture and layout form. In accordance with the latest state regulations (GB50180-2018), which are based on comprehensive research results, and which contain the relevant specifications, the maximum height limit for high-rise buildings was been restricted to 80 m. As demonstrated in Figure 2b, the main heights of the residences were between 18 and 24 storys.

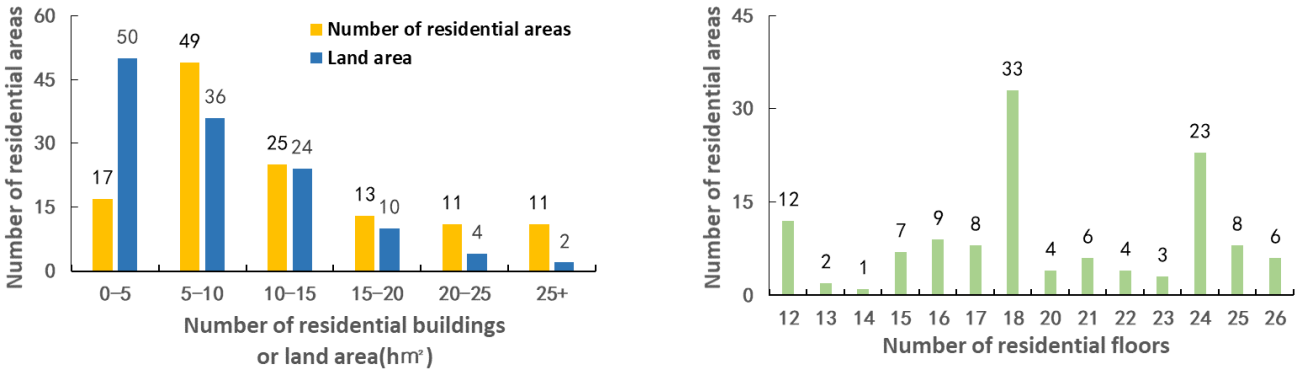

Figure 2. High-rise residential buildings in Harbin. (**a**) Distribution of land area and number of buildings and (**b**) distribution of height of buildings.

2.2. Mock Object

To reflect the influence of building height and layout on the vertical wind environment on building surfaces, the model needed to be arranged in groups, so that the vertical influence of the wind on each building in the model was as comprehensive as possible. First, in accordance with the latest national standard (GB50180-2018), the spatial scale of the study was defined at the neighborhood block level, with an area of 2–4 ha. In addition, based on the area with the largest distribution of residential land in Harbin, indicated in Figure 2a, it was decided that the length and width of the simulation scale should be 220 m and 2 ha, respectively. Second, based on the number of buildings included in a single group of residential land in Harbin as indicated in Figure 2a, the number of simulated buildings chosen was 9. Finally, based on the height distribution of residential buildings in Harbin, as indicated in Figure 2b, the heights of two typical buildings were set at 18 and 24 storys. The length, width, and height of the individual buildings were set in accordance with the GB50096-2011 specifications. A single building was 60 m in length, 15 m in width, and 3 m in height. The building spacing was selected in accordance with the specifications of Harbin's Urban and Rural Planning Regulations for sunlight and fire spacing [29]; that is, where the height of the building on the south side was H, the relative spacing of the longitudinal wall was 1.2 H, and that of the gable was 20 m. The specific spacing of buildings is indicated in Figure 3.

Because Harbin is situated in a cold climate, the residential buildings have higher requirements for sunshine exposure, and the low height of winter sun results in the need to space building further apart to accommodate the requirements for sunshine space. To improve land use efficiency, developers tend to construct low-height buildings on the south side, and high-height buildings on the north side, which was also reflected in the survey results. In this study, regional layout characteristics were considered to reduce the need for special working conditions. Therefore, the south-side height characteristic

was excluded, and seven building height distribution modes were selected: as the control group, the seven building height distribution modes relating to uniform building height (UBH) and non-uniform building height distribution modes of the north side height (1-N), east side height (1-E), west side height (1-W), east and north side height (2-EN), west and north side height (2-WN), and east and west side height (3-EWN) are shown in Figure 3. Finally, to reduce the influence of irrelevant factors, all buildings were laid out in rows in a north–south direction.

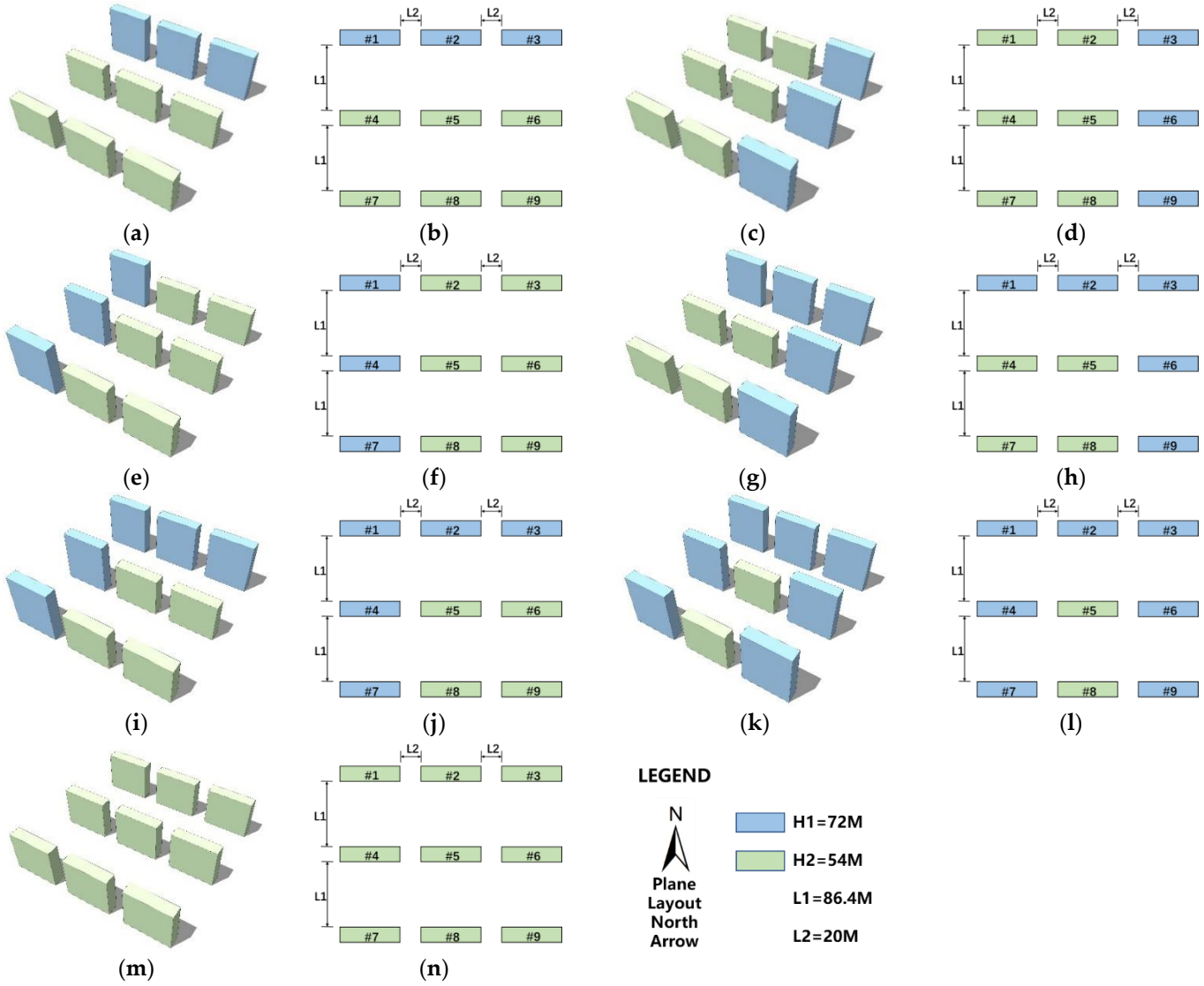

Figure 3. Schematic diagram showing building height, spacing, numbering, and 3D model of seven building distribution patterns: (**a**) north side high (1-N) 3D model, (**b**) north side high (1-N) plan layout, (**c**) east side high (1-E) 3D model, (**d**) east side high (1-E) plan layout, (**e**) west side high (1-W) 3D model, (**f**) west side high (1-W) plan layout, (**g**) east and north side high (2-EN) 3D model, (**h**) east and north side high (2-EN) plan layout, (**i**) west and north side high (2-WN) 3D model, (**j**) west and north side high (2-WN) plan layout, (**k**) east–west and north side high (3-EWN) 3D model, (**l**) east west and north side high (3-EWN) plan layout, (**m**) uniform building height (UBH) 3D model, and (**n**) uniform building height (UBH) plan layout.

2.3. Boundary Conditions

Common CFD simulation software includes Airpak, Pheonics, Wind Perfect, Star-CD, and Fluent. Pheonics has simple and intuitive parameter settings, can automatically generate and adjust grids, and makes use of rich calculation models, thereby performing

efficient simulations. Its FLAIR module is specially designed for the simulation of the wind environment to inform the grouping and distribution of outdoor buildings. Numerous studies in recent years have verified its accuracy and reliability in wind environment simulation [18,30]. Therefore, this study has used the Pheonics 2019 software based on the Reynolds average equation and Sketchup2018 to generate a 3D model of the simulated area, as shown in Figure 3.

2.3.1. Air Velocity Setting

In the simulation, the vertical air flow level at the entrance usually appeared lower, however regional terrain can also influence this, thereby producing a corresponding change. The influence of friction because of terrain results in a decrease in air velocity and can also produce the vertical air exchange function. Air velocity decreases with an increase in height, and is not affected by surface roughness in the atmospheric boundary layer; as such, free air flow is restored. As shown in Figure 4, this study utilized the Harbin air velocity, wind direction, and atmospheric pressure data obtained from The National Climatic Data Center (NCDC) of the United States [31]. Data collected from 1956 to 2020 at 3 h intervals were used. The average wind speed in Harbin is 3.23 m/s, the average atmospheric pressure is 100,553.8 Pa, and the prevailing wind direction is SSW. The above data were manually entered into the Phoenics wind environment attribute interface and are shown in Figure A1 under Appendix A.

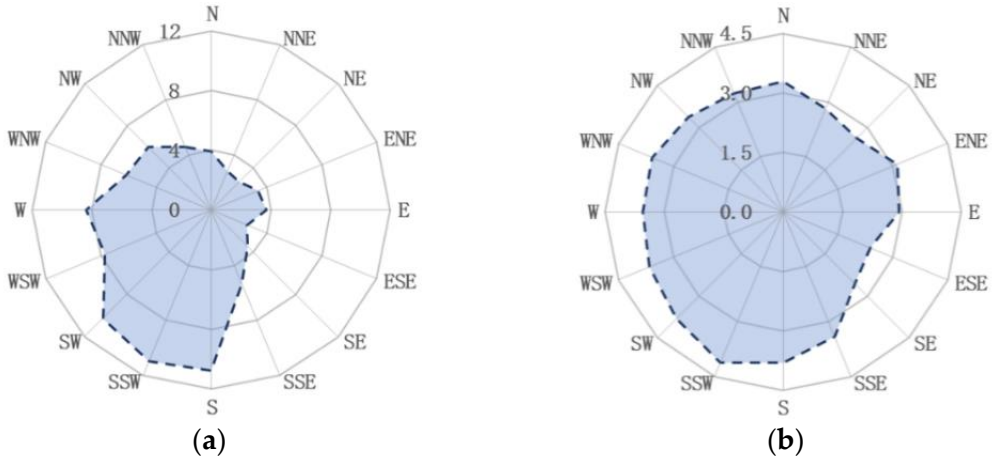

Figure 4. Harbin air velocity and frequency statistics map showing (**a**) air velocity statistics and (**b**) wind frequency statistics.

2.3.2. Mean Air Velocity Distribution

Because of the influence of surface friction on air velocity, the variation law of average air velocity in the atmospheric boundary layer with the change of height can be expressed in two forms: exponential law and logarithmic law. The exponential law is derived from the actual measurement results, and the logarithmic law is derived from the boundary layer theory. In this study, the exponential law was used to calculate the change in air velocity near the surface, and the formula is as follows:

$$u = U_0 \left(\frac{Z}{Z_0} \right)^a \quad (1)$$

In this formula, Z_0 is the standard height above ground, which is generally 10 m. The incoming flow velocity at this height is U_0, Z is the variable height from the ground, u is the air velocity at this height, and α is the roughness coefficient of the ground [32]. The subject of this study falls within the standard definition of urban building density as defined in the Thermal Environment Design Standard for Urban Residential Areas (JGJ286-2013); as such,

the roughness coefficient(α) is 0.22 [33]. Specific parameters were manually entered into the Phoenics wind environment attribute interface, as shown in Figure A1.

2.4. Domain Size

The size of the computational domain could affect the reliability of the simulation experiment results. In accordance with the requirements of wind tunnel tests, the clogging rate of the computational domain should be kept below 3%, which is generally defined as the ratio of the frontal area of working conditions to the vertical cross-sectional area of the computational domain [34,35]. Relevant experimental cases have demonstrated that the lateral and upper boundaries should be greater than or equal to 5 H, where H is the maximum building height and therefore the outflow boundary should be set at the rear of the building to at least 10 H and consistent with the wind direction [36,37]. In addition, the height determination of the computational domain is also affected by different terrain type distribution. Based on the defined parameters and combined with wind direction, the respective longitudinal (Y), transverse (X), and vertical (Z) extents for this study were calculated to be 1297 m, 1300 m, and 432 m, respectively, as shown in Figure A2 under Appendix A. The dimensions on the XY plane are indicated in Figure A3 under Appendix A, and are 10 H in the eastern and northern directions, and 5 H in the western and southern directions. As shown in Figure A4 under Appendix A, the height on the Z plane is 5 H.

2.5. Grid Size and Independence

Grids of different scales are required for computing domains and core areas. To clearly express the vertical wind speed distribution, the Z-axis grid was set to a building height of 3 m, as shown in Figure A5c under Appendix A. As shown in Figure A5a,b, two grids were used for the X-axis and Y-axis, 15 m in the computational domain and 5 m in the core area, respectively, to meet the requirements of the horizontal and vertical proportions of the grid cells. The mesh setting was refined towards the core area and subdivided using SPARSOL to ensure statistical accuracy (Figures A2 and A5). Grid independence verification indicated that the difference in simulation results was less than 5% when the grid scale was doubled, hence the research grid met the requirements without requiring further encryption.

2.6. Solution Methods and Convergence Condition

The standard *K*-ε model was used to calculate turbulence. This model has a reasonable prediction capability in a large turbulence range and is widely used in practical engineering [38]. To ensure accuracy and convergence of the results, it is generally required that the simulation residual of all working conditions reaches 10^{-4} or less [39,40]. The Phoenics settings required for this study are shown in Table 1. As shown in Figure A6 under Appenidx A, the number of simulation iteration steps for the seven layout methods was 20,000 and the residual error was maintained below 10^{-5}.

Table 1. Phoenics simulation condition settings.

Computing Elements	Set the Content
Computation domain size	1297 × 1300 × 432 m
Core area grid size	X-axis and Y-axis are 5 m, and the z-axis is 3 m
Turbulence model	Standard K-ε turbulence model
Flow speed	3.23 m/s, height 10 m
Flow direction	Prevailing wind direction SSW in Harbin (202.5°)
Experimental algorithm	SIMPLE
Convergence condition	Maximum allowable residual of 10^{-5}
Iteration steps	20,000

2.7. Validation of the CFD Simulation

One of the purposes of this study was to verify the influence of a non-uniform layout of high-rise buildings on the vertical wind environment. Therefore, the layered sampling method was adopted to sample the height of buildings in Harbin and conduct modeling

on the non-uniform layout, to create the wind tunnel test conditions shown in Figure 5. The same operating conditions used in the preceding CFD simulation were used and the results were compared to the relevant town planning specifications (JGJ/T338-2014 and JTG/T3360-01-2018) [41,42]. The results can be considered to concur if the air velocity error between the numerical simulation and wind tunnel test at the same position is less than 10% within the same boundary parameters. Specific verification results are provided in Section 3.1.

Figure 5. Wind tunnel test site layout.

2.8. Simulation Results Evaluation Criteria

The wind environment needed to be simulated for the abstract models of seven height distribution modes using the parameters described above and then the ParaView5.10 software was used to export and process the air velocity and wind pressure data.

When evaluating air velocity, the Beaufort Wind Scale correlated the influence of air velocity on people, as shown in Table 2 [43]. As a city typical of colder regions, Harbin is required to meet the green building evaluation standard (GB/T50378-2019) for pedestrian zone air velocity of less than 5 m/s in winter [44]. Low wind speed can lead to poor air circulation and long-term accumulation of pollutants, thereby affecting people's comfort and health. Research that observed the effects of air velocity on the human body, as shown in Table 2, indicates that regions with air velocity lower than 1 m/s or 0.5 m/s can be defined as calm wind zones [45,46].

Table 2. Evaluation standard for the correlation between air velocity and comfort.

Wind Level	Air Velocity Range (m/s)	Effects on the Human Body
0	$0 < V \leq 0.1$	Stuffy
1	$0.1 < V \leq 1$	Imperceptible
2	$1 < V \leq 2.1$	Light breeze
3	$2.1 < V \leq 3.4$	Disheveled hair
4	$3.4 < V \leq 5$	Excessive dust
5	$5 < V \leq 6.7$	Tolerable limit for onshore wind
6	$6.7 < V \leq 8.6$	Difficulty walking and holding an umbrella

When evaluating wind pressure, barring the first row of windward buildings, the wind pressure difference between the windward side and the leeward side of each building should not be greater than 5 Pa [47]. It is also necessary to ensure that more than 75% of concrete buildings have a 1.5 Pa wind pressure difference between the windward side and the leeward side [48].

The above evaluation was based on pedestrian height. In a natural ventilation state, the comfort of each floor of a high-rise building is related to the pedestrian height. Therefore, the evaluation of air velocity and wind pressure is also applicable in the vertical direction. That is, the acceptable air velocity is 1–5 m/s, and the acceptable wind pressure difference ranges from ±1.5–5 Pa.

The effects on thermal comfort caused by ventilation were evaluated in this study using the Universal Thermal Climate Index (UTCI) to express the comfort effect of different vertical wind speed distributions on people who open windows for ventilation [49,50]. The formula is:

$$UTCI = f(R_h, T_{mrt}, V_a, T_d) \quad (2)$$

where R_h is the air humidity, T_{mrt} is the mean radiation temperature, V_a is the wind speed, and T_d is the air temperature [49]. The UTCI calculation was performed using the Grasshopper script. The Harbin T_d data originated from the statistical data of the NCDC [31] where the average temperature is 4.67 °C, the suitable human R_h humidity is 50% [50], and the T_{mrt} is the average radiation temperature of 24 °C [51]. As shown in Table 3, different UTCI ranges represent cold or hot regions and this research was carried out by modifying the range in line with the characteristics of cold regions [52].

Table 3. UTCI original standard and cold region modified standard.

UTCI (°C) Range [53]	Cold Land UTCI (°C) Range Correction [52]	Stress Category on the Human Body
+38 to +46	+39 to +45	Very strong heat stress
+32 to +38	+33 to +39	Strong heat stress
+26 to +32	+21 to +33	Moderate heat stress
+9 to +26	+3.5 to +21	No thermal stress
+9 to 0	+3.5 to −4	Slight cold stress
0 to −13	−4 to −11	Moderate cold stress
−13 to −27	−11 to −18	Strong cold stress

3. Results and Analysis

3.1. CFD Simulation Verification Results

As shown in Figure 6, the air velocity data extracted from the wind tunnel test is presented as a line graph with the power function fitted for processing followed by performing an error calculation using the data generated from the Phoenics simulation. The point selection error and curve (CFD simulation curve and wind tunnel fitting curve comparison) errors were distributed in the range of −4–9%, which are all lower than the 10% specification requirement. Therefore, the reliability of the CFD simulation data was found to be high, and subsequent simulation analyses could be performed. The specific processing method began with the extraction of air velocity and wind pressure data from the grid nearest to the building surface. Based on the number of grids covered by the building surface, the average air velocity and wind pressure at the corresponding height was taken based on a building unit height of the number of storys. Finally, the distribution of windward and leeward air velocity, windward and leeward wind pressure, and wind pressure differences at each building was formed.

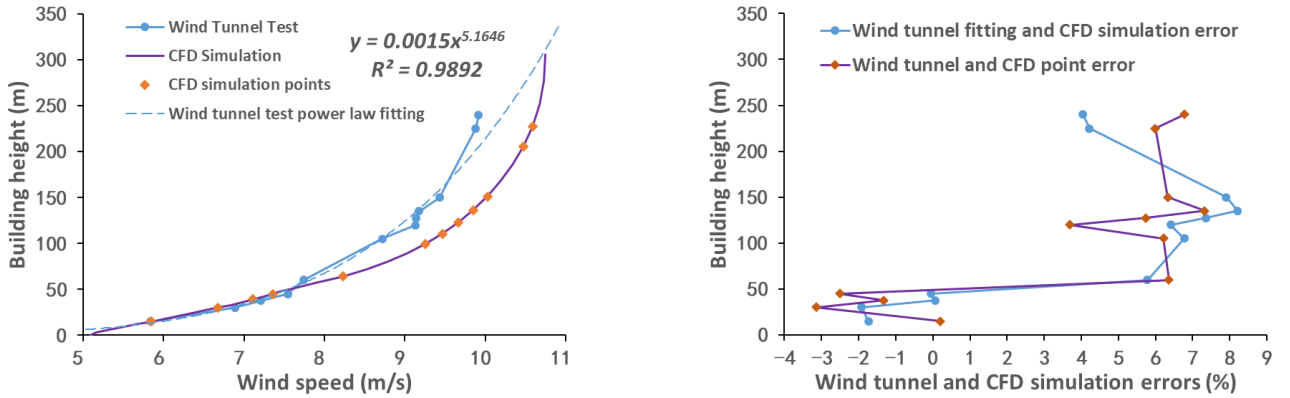

(**a**) (**b**)

Figure 6. Wind tunnel test, air velocity CFD simulation, and error distribution. (**a**) Air velocity distribution and (**b**) Error distribution.

3.2. Air Velocity Influence

Figure 7 and Table 4 show the proportion of air velocity distribution on building surfaces in seven distribution patterns. The simulation parameters were set according to the parameters outlined in Table 1. Figure 8 indicates the air velocity distribution on the building surface and the main vertical sections between buildings #2, #5, and #8 in seven distribution patterns.

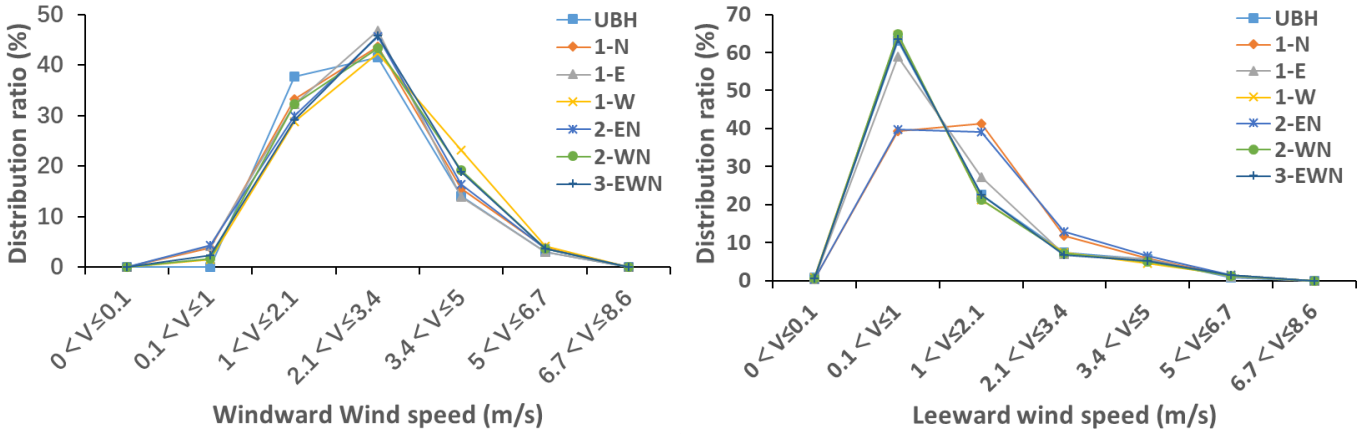

(**a**) (**b**)

Figure 7. Proportional distribution of air velocity for seven building distribution patterns. (**a**) Windward side of the building and (**b**) leeward side of the building.

Table 4. Air velocity proportions for seven building distribution patterns.

Air Velocity Distribution (m/s)		The Proportion of Air Velocity Distribution (%)						
		UBH	**1-N**	**1-E**	**1-W**	**2-EN**	**2-WN**	**3-EWN**
Windward air velocity (m/s)	$0 < V \leq 0.1$	0.00	0.00	0.00	0.00	0.00	0.00	0.00
	$0.1 < V \leq 1$	0.04	3.83	4.07	1.51	4.29	1.61	2.35
	$1 < V \leq 2.1$	37.79	33.29	32.23	28.77	30.04	32.22	29.22
	$2.1 < V \leq 3.4$	41.52	43.63	46.81	42.41	45.62	43.44	45.79
	$3.4 < V \leq 5$	14.04	15.51	13.92	23.12	16.38	19.14	18.92
	$5 < V \leq 6.7$	2.97	3.74	2.97	4.19	3.67	3.60	3.72
	$6.7 < V \leq 8.6$	0.00	0.00	0.00	0.00	0.00	0.00	0.00

Table 4. *Cont.*

Air Velocity Distribution (m/s)		The Proportion of Air Velocity Distribution (%)						
		UBH	1-N	1-E	1-W	2-EN	2-WN	3-EWN
Leeward air velocity (m/s)	$0 < V \leq 0.1$	0.67	0.37	0.37	0.73	0.38	0.57	0.58
	$0.1 < V \leq 1$	63.02	39.28	58.81	64.71	39.72	64.87	63.45
	$1 < V \leq 2.1$	22.67	41.23	27.23	21.29	39.11	21.24	22.64
	$2.1 < V \leq 3.4$	7.29	11.88	6.96	7.37	12.78	7.12	6.75
	$3.4 < V \leq 5$	5.67	5.94	5.66	4.56	6.47	4.94	5.09
	$5 < V \leq 6.7$	0.67	1.30	0.98	1.34	1.53	1.26	1.48
	$6.7 < V \leq 8.6$	0.00	0.00	0.00	0.00	0.00	0.00	0.00

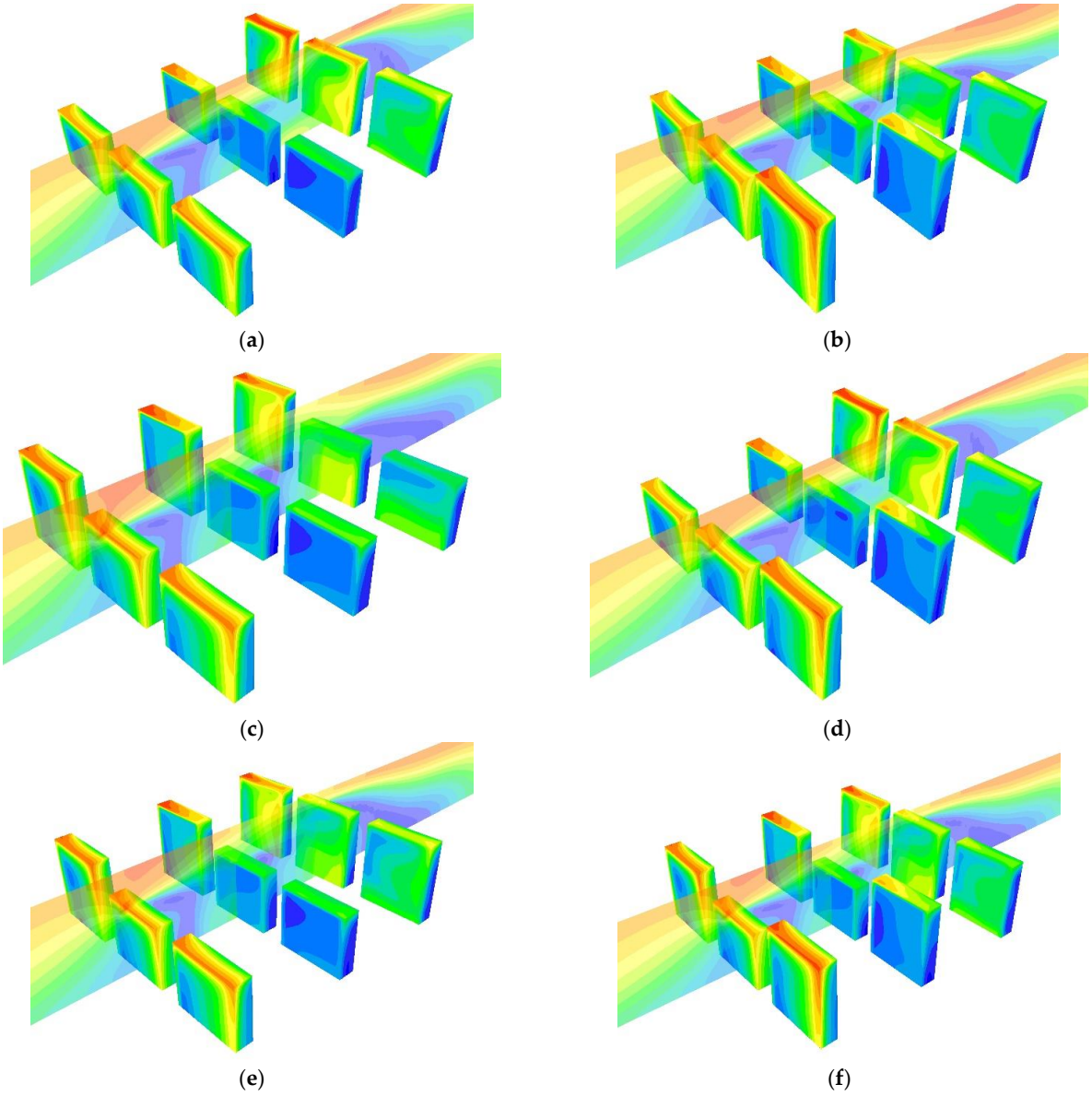

Figure 8. *Cont.*

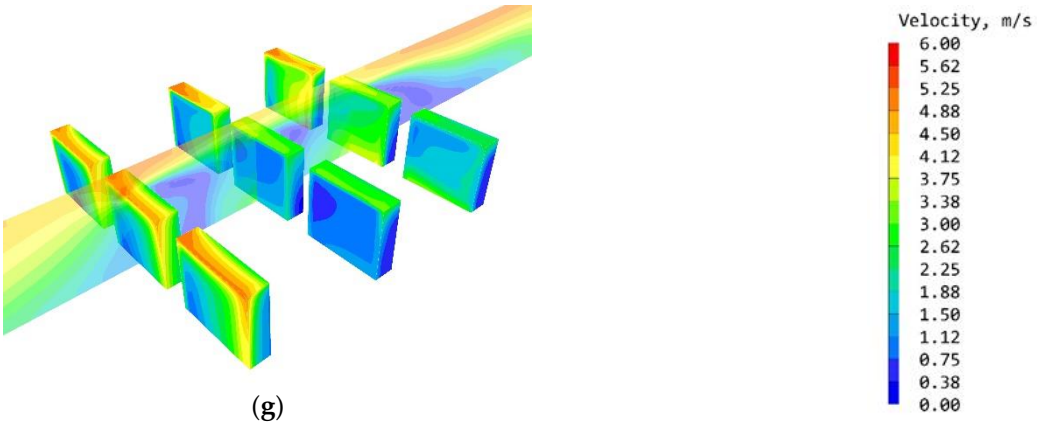

(**g**)

Figure 8. Three-dimensional air velocity map for seven building distribution patterns. (**a**) North side high (1-N), (**b**) east side high (1-E), (**c**) west side high (1-W), (**d**) east and north side high (2-EN), (**e**) west and north side high (2-WN), (**f**) east–west and north side high (3-EWN), and (**g**) uniform building height (UBH).

3.2.1. Windward Air Velocity

It is evident from the statistical results that the main air velocity distributions of the seven distribution modes were between 2.1 and 3.4 m/s and the distribution ratio of comfortable air velocity in all distribution modes could reach more than 90%. However, there were 2.97–4.19% air velocities that were statistically greater than 5 m/s, which were all located at the upper and side gables of the buildings. There are no windows in these parts of the buildings, therefore these velocities would have little impact on the overall comfort.

According to the statistical results for each building shown in Figure A7, the average air velocity of buildings #1 and #4 on the windward side under the roof had a low variation range, and rapidly recovered to more than 5 m/s on the top floor of the building. The air velocities at buildings #7, #8, and #9, on the main windward side, changed with the increase of height. The air velocity at building #8 on the east side, which was high (1-E), decreased with the increase in height under the influence of the corner flow zone on the east side, with a decrease of 1.43 m/s. The air velocity at buildings #8 and #9, which were high (1-W) on the west side, decreased by 0.8 m/s and 1.63 m/s under the influence of the corner flow zone on the west side.

The buildings on the non-windward side were sheltered by the front and side buildings, and the average air velocity change mainly decreased with the increase in height. Among them, three buildings on the east side had a layout pattern with taller buildings, 1-E, 2-EN, and 3-EWN, and a slight decrease and then rise in air velocity was observed at building #6. The air velocity at buildings #2 and #3, which were downwind, increased when the building on the west side was high, and the increase was found to be significantly correlated to the increase of height.

3.2.2. Leeward Air Velocity

As the statistical results demonstrated, the main leeward air velocity distribution of the seven distribution modes was 0.1–1.0 m/s, which falls within the low air velocity category. Each distribution mode had a windless area of at least less than 0.67% and these spaces were prone to poor air circulation. The proportion of air velocity in the 1–5 m/s zone of comfort was 33.21–35.63%, and the two downwind modes, 1-N and 2-EN, of the building layout experienced a better ventilation effect on the leeward side of the building, accounting for 59.06 and 58.36%, respectively.

According to the statistical results shown in Figure A8, the average leeward air velocity of the nine buildings was strongly consistent with the change in height. Most of the buildings had low initial air velocity, and the air velocity increased slightly with the increase in height. The air velocity at the roof position was close to or exceeded the incoming air

velocity of 3.23 m/s. An important trend was observed at buildings #5 and #6 with two layouts, 1-N and 2-EN, of the north height and east north height. In both cases, the initial air velocity was in the appropriate range and decreased with the increase in height with the air velocity being highest at the top.

3.3. Wind Pressure Effect

Figure 9 and Table 5 show the distribution ratio of building surface wind pressure under seven distribution patterns. Figure 10 shows the wind pressure on the building surface and main vertical sections, between buildings #2, #5, and #8, under seven distribution modes. The simulation parameters were set according to the parameters outlined in Table 1.

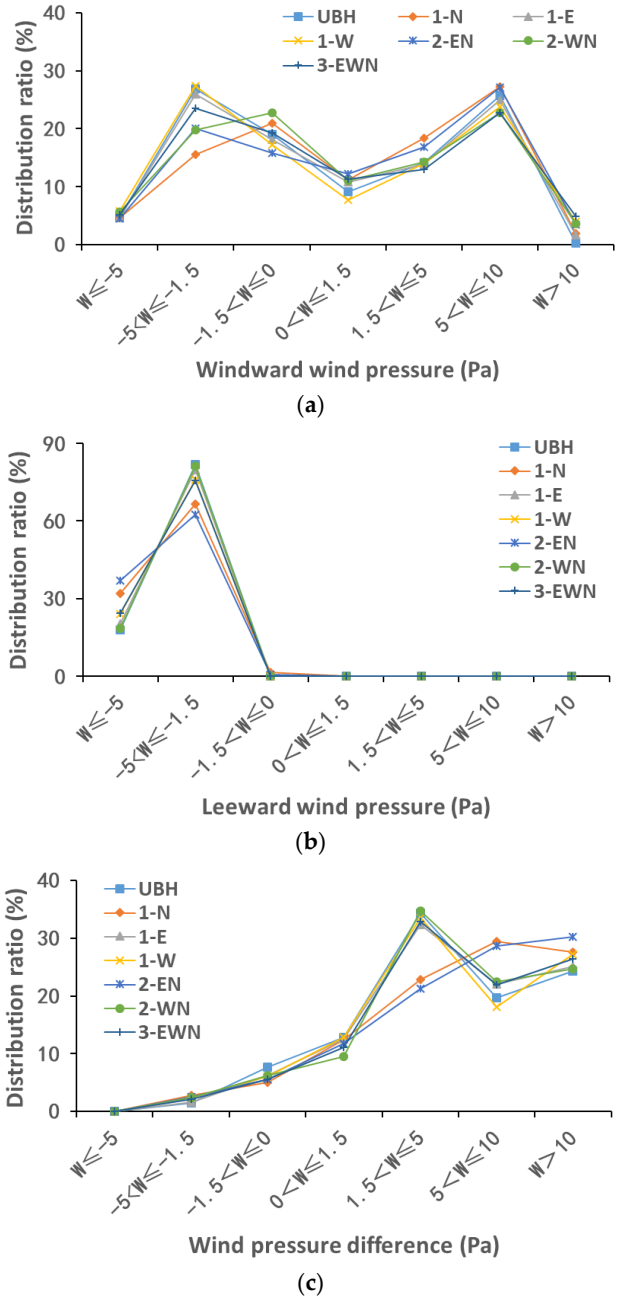

Figure 9. Proportional distribution of wind pressure for the seven building distribution patterns. (**a**) Windward pressure at the building, (**b**) leeward pressure at the building, and (**c**) wind pressure difference at the building.

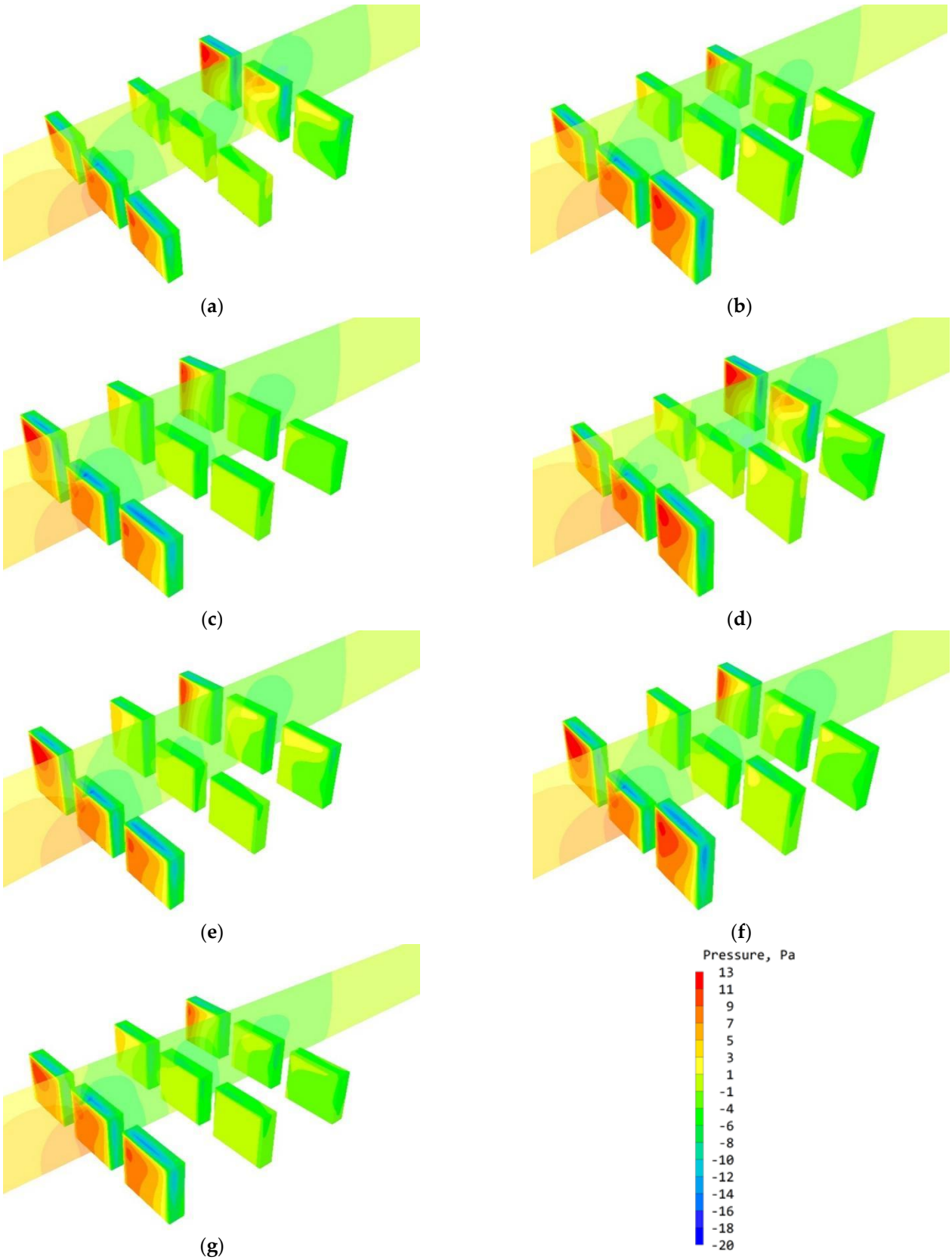

Figure 10. Three-dimensional wind pressure map of seven building distribution patterns. (**a**) North side high (1-N), (**b**) east side high (1-E), (**c**) west side high (1-W), (**d**) east and north side high (2-EN), (**e**) west and north side high (2-WN), (**f**) east–west and north side high (3-EWN), and (**g**) uniform building height (UBH).

Table 5. Wind pressure ratios of seven building distribution modes.

Wind Pressure Distribution (Pa)		The Proportion of Wind Pressure Distribution (%)						
		UBH	1-N	1-E	1-W	2-EN	2-WN	3-EWN
Windward wind pressure (Pa)	$W \leq -5$	4.77	4.60	4.64	5.82	4.52	5.70	5.13
	$-5 < W \leq -1.5$	26.90	15.59	25.97	27.43	20.05	19.82	23.58
	$-1.5 < W \leq 0$	19.03	21.00	18.11	17.26	15.81	22.73	19.32
	$0 < W \leq 1.5$	9.09	11.15	10.83	7.69	12.17	11.06	11.38
	$1.5 < W \leq 5$	14.13	18.44	13.84	14.04	16.84	14.27	13.04
	$5 < W \leq 10$	25.78	27.27	24.91	23.77	27.13	22.77	22.72
	$W > 10$	0.31	1.95	1.71	3.99	3.48	3.64	4.84
Windward wind pressure (Pa)	$W \leq -5$	18.04	32.03	20.31	23.97	36.85	18.64	24.23
	$-5 < W \leq -1.5$	81.87	66.50	79.69	76.03	62.46	81.36	75.77
	$-1.5 < W \leq 0$	0.09	1.47	0.00	0.00	0.69	0.00	0.00
	$0 < W \leq 1.5$	0.00	0.00	0.00	0.00	0.00	0.00	0.00
	$1.5 < W \leq 5$	0.00	0.00	0.00	0.00	0.00	0.00	0.00
	$5 < W \leq 10$	0.00	0.00	0.00	0.00	0.00	0.00	0.00
	$W > 10$	0.00	0.00	0.00	0.00	0.00	0.00	0.00
Wind pressure difference (Pa)	$W \leq -5$	0.00	0.00	0.00	0.00	0.00	0.00	0.00
	$-5 < W \leq -1.5$	1.44	2.73	1.63	2.32	2.49	2.41	2.09
	$-1.5 < W \leq 0$	7.60	5.05	6.27	6.11	5.59	6.28	5.60
	$0 < W \leq 1.5$	12.78	12.45	12.58	12.78	11.79	9.49	11.16
	$1.5 < W \leq 5$	34.28	22.79	32.36	33.54	21.28	34.75	32.83
	$5 < W \leq 10$	19.66	29.43	22.10	18.03	28.66	22.43	21.92
	$W > 10$	24.25	27.55	25.07	27.23	30.20	24.65	26.40

3.3.1. Windward Wind Pressure

The significance of single-side wind pressure statistics was influenced by interior corridor layout where ventilation of all rooms cannot be guaranteed by the pressure difference on the windward and leeward sides of the building itself. Therefore, pressure on one side of the building could also improve ventilation and increase spatial comfort.

As evidenced by the overall wind pressure distribution presented in Figures 9a and 10, the high wind pressure distribution on the windward side was mostly concentrated on the windward buildings of the seven layout modes and the high pressure distribution was also present at the lateral windward buildings. The distribution of wind pressure in the acceptable range was above 78% with the highest being 85.83% (UBH) and the lowest 78.66% (3-EWN).

According to the average windward wind pressure of buildings shown in Figure A9, the wind pressure of the windward buildings in the first row, buildings #7, #8, and #9, changed considerably. The wind pressure decreased rapidly and became negative as the building height approched the top floor. Notable observations were made in the case of building #8 with east side high (1-E) and west side high (1-W), and building #9 with west side high (1-W) and east and north side high (2-EN). The initial wind pressure was negative and the variation range was small. The wind pressure at the center-row buildings #4, #5, and #6 varied slightly. The initial wind pressure was −1.91–1.0 Pa, and the maximum negative wind pressure was observed on the top floor of the building. The rear buildings #1, #2, and #3 were substantially affected by the layout and the initial wind pressure changes. Building #2, west side high (1-W), had the largest initial wind pressure, which was 5.37 and 4.42 Pa respectively. The wind pressure changes were the most elevated at a height above 42 m.

3.3.2. Leeward Wind Pressure

According to the results presented in Figure 9b and Table 4, the wind pressure on the leeward side was principally negative, and its distribution ranged from 62.46–81.87%, which was within the acceptable range. The acceptable wind pressure distribution of the

north side high (1-N) and east and north high (2-EN) was 66.5% and 62.46%, respectively, with few distributions. This indicated that the layout of high-rise buildings downwind was not conducive to creating appropriate leeward wind pressure. The negative wind pressure was greater than 5 Pa for all layout patterns, and the distribution proportion were 18.04–36.85%. The high proportion was observed in the north side high (1-N) and east and north high (2-EN) areas, which were 32.03% and 36.85%, respectively.

Figure A10 presents the average wind pressure on the leeward side of the buildings. The wind pressure of the seven layout modes was less affected by the change in height and was mainly stable. The center row buildings #4, #5, and #6 varied substantially with the layout pattern of high-rise buildings on the rear and lateral rear (1-N and 2-EN).

3.3.3. Wind Pressure Difference

According to the results presented in Figure 9c and Table 4, overall, a wind pressure difference of 1.5 Pa before and after 75% could be achieved for all the seven distribution modes, and the distribution ratio ranged from 79.62–84.23%. However, the optimum wind pressure distribution of each distribution mode was not more than 38%, and ranged from 23.77–37.16%. At the same time, there were areas with a wind pressure difference greater than 5 Pa, accounting for 43.90–58.86%. In these areas, it was necessary to strengthen windproofing at the building entrance to prevent heat loss as a result of air egress and to reduce the wind pressure differences to stabilize indoor and outdoor ventilation to meet human comfort needs.

As indicated in Figure A11, the initial average wind pressure difference between the front and rear of the first row of windward buildings #7, #8, and #9 was large, with a range of 8.31–10.12 Pa. An important observation was made in the case of building #8, where the pressure was high on the east (1-N) and high on the west (1-W), and building #9, which was high on the west (1-W) and high on the east and north (2-EN). The wind pressure difference was negative and small, and the variation range was small as height increased. The center row buildings #4, #5, and #6 had a small wind pressure variation range. Building #4 faces the wind laterally and the average distribution of wind pressure difference for the building was slightly higher. Buildings #5 and #6 had an average wind pressure difference within the acceptable comfort zone. The layout influenced the initial wind pressure difference between rear row buildings #1, #2, and #3, which changed substantially. The roof wind on front row buildings influenced the average wind pressure differences at buildings #1 and #2 with the layout pattern of rear-row taller buildings (1-N and 2-EN) changing substantially with the increase in height. Building #2 and #3, which are located in the west side high (1-W) layout, are blocked by the west side high-rise buildings, showed the largest initial wind pressure difference of 9.80 and 9.30 Pa, respectively, and the variation range of wind pressure difference was the largest from a height of 42 m.

3.4. UTCI Thermal Comfort Assessment

Figure 11 indicates the UTCI proportion distribution of each building surface under the seven distribution modes, and the statistical value of the excluded interval was 0. Table 6 presents the overall distribution proportion of the UTCI interval on the building surface of the seven distribution modes.

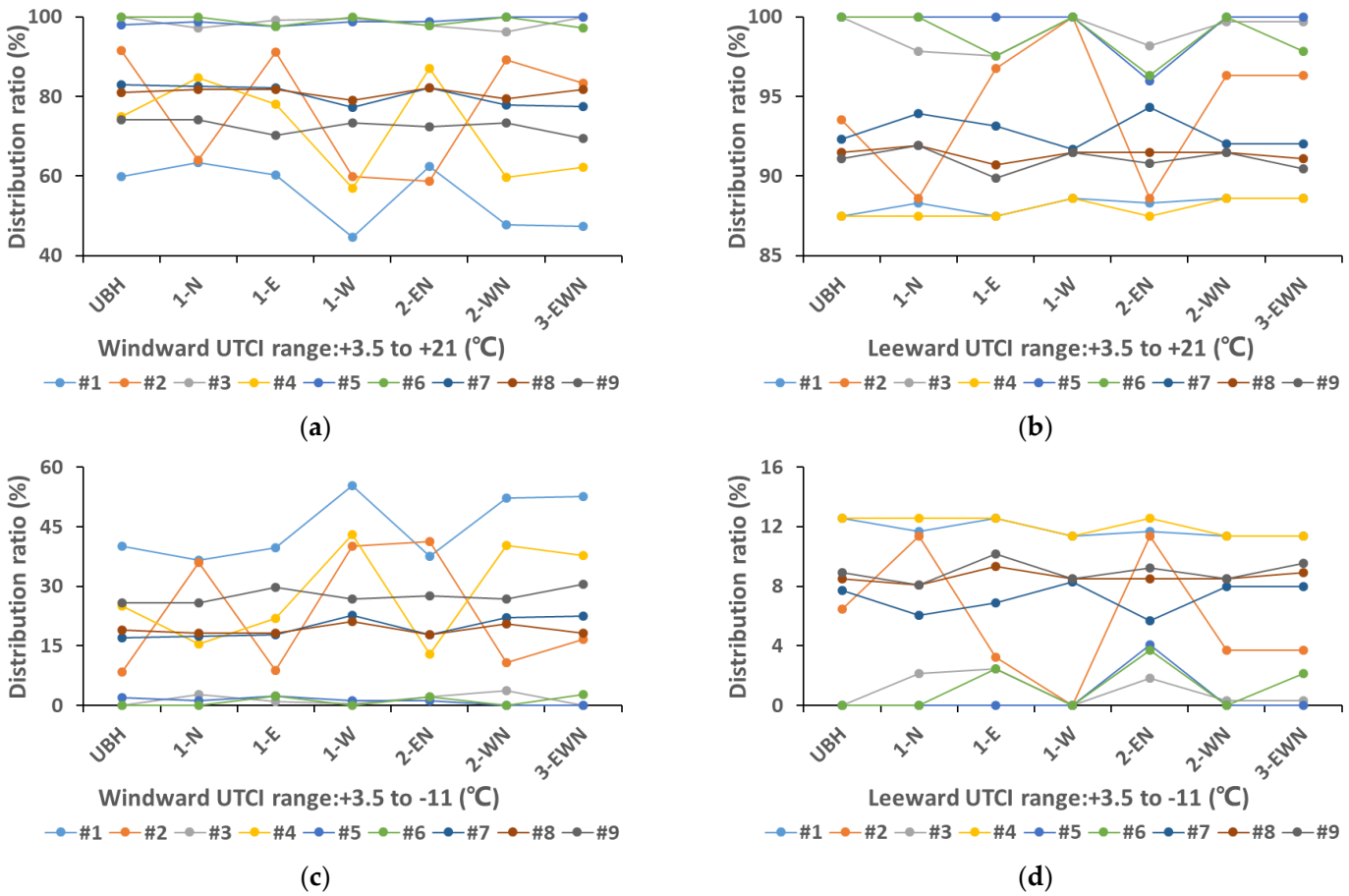

Figure 11. Proportion distribution of UTCI interval of seven building distribution patterns. (**a**) Windward UTCI no thermal stress zone, (**b**) leeward UTCI no thermal stress zone, (**c**) windward UTCI slight/moderate cold stress zone, and (**d**) leeward UTCI slight/moderate cold stress zone.

Table 6. Distribution table of UTCI ratio of seven building distribution modes.

Universal Thermal Climate Index (°C)		The Proportion of Universal Thermal Climate Index (UTCI) Distribution (%)						
		UBH	1-N	1-E	1-W	2-EN	2-WN	3-EWN
Windward UTCI (°C)	+39 to +45	0.00	0.00	0.00	0.00	0.00	0.00	0.00
	+33 to +39	0.00	0.00	0.00	0.00	0.00	0.00	0.00
	+21 to +33	0.00	0.00	0.00	0.00	0.00	0.00	0.00
	+3.5 to +21	84.71	82.17	84.66	74.97	81.52	79.45	79.27
	+3.5 to −4	15.29	17.46	14.98	25.03	17.91	20.55	20.40
	−4 to −11	0.00	0.37	0.37	0.00	0.57	0.00	0.33
	−11 to −18	0.00	0.00	0.00	0.00	0.00	0.00	0.00
Leeward UTCI (°C)	+39 to +45	0.00	0.00	0.00	0.00	0.00	0.00	0.00
	+33 to +39	0.00	0.00	0.00	0.00	0.00	0.00	0.00
	+21 to +33	0.00	0.00	0.00	0.00	0.00	0.00	0.00
	+3.5 to +21	93.70	93.16	93.53	94.18	92.38	94.07	93.75
	+3.5 to −4	6.30	6.84	6.47	5.82	7.58	5.93	6.25
	−4 to −11	0.00	0.00	0.00	0.00	0.04	0.00	0.00
	−11 to −18	0.00	0.00	0.00	0.00	0.00	0.00	0.00

According to the results presented in Table 4, UTCI comfort on the leeward side was better than that on the windward side, with a difference of 9–19.3%. The largest difference occured in the layout mode with the height on the west side. The amount of space with high degrees of comfort exceeded 74.9% and on the leeward side was more than 92%, indicating that natural ventilation could improve the spatial extent of comfort. However, 14.9–25%

of the space was located in a slightly colder stress area, which needed to be mitigated by installing mechanical ventilation or window shielding.

Based on the UTCI proportional distribution of buildings, presented in Figure 11a,b, on the windward side, the comfort zone, +3.5 °C to +21 °C of each building had a distribution proportion higher than 60%, and buildings #1, #2, and #4 were most affected by height, with a variation range of 18.77%, 32.73%, and 27.35%. Buildings #3, #5, and #6 had the highest proportion of comfort zones, and all layouts could improve comfort. Windward buildings #7, #8, and #9 had a higher proportion of comfort distribution, 69.5–82.9%, with limited layout effects. The comfort zones on the leeward side were all above 87.4%, and only building #2 was substantially affected by the layout change, which changed by 11.38%.

As shown in Figure 11c,d, the distribution proportion of the slight/moderate cold stress factor on the windward side was mostly below 30%. Buildings #1, #2, and #4 were substantially affected by height change and building #1 had the highest distribution variation range of 36.6–55.4%. The distribution proportion of the slight/moderate cold stress factor on the leeward side was less than 13% and only building #2 was significantly affected by the layout.

3.5. Layout Rationality Judgment

According to the ranking logic shown in Table 7, by studying the distribution of wind speed, wind pressure, and UTCI parameters of 9 buildings in 7 layout modes, the distribution percentages of different ranking intervals were calculated respectively, and then the ranking and summation were carried out to form the wind environment and UTCI parameters of the 9 buildings, as shown in Figure A12. On this basis, the overall comfort level of seven distribution modes has been ranked.

Table 7. Sort range and sort description of wind environment and UTCI parameters.

Sort Range		Sort Description
Air velocity (m/s)	$0 < V \leq 0.1$	Lower interval percentage correlates to higher sorting.
	$0.1 < V \leq 1$	
	$1 < V \leq 2.1$	
	$2.1 < V \leq 3.4$	Higher interval percentage correlates to higher sorting.
	$3.4 < V \leq 5$	
	$5 < V \leq 6.7$	Lower interval percentage correlates to higher sorting.
	$6.7 < V \leq 8.6$	
Wind pressure (Pa)	$W \leq -5$	Lower interval percentage correlates to higher sorting.
	$-5 < W \leq -1.5$	Higher interval percentage correlates to higher sorting.
	$-1.5 < W \leq 0$	Lower interval percentage correlates to higher sorting.
	$0 < W \leq 1.5$	
	$1.5 < W \leq 5$	Higher interval percentage correlates to higher sorting.
	$5 < W \leq 10$	Lower interval percentage correlates to higher sorting.
	$W > 10$	
Universal Thermal Climate Index (°C)	+39 to +45	
	+33 to +39	Lower interval percentage correlates to higher sorting.
	+21 to +33	
	+3.5 to +21	Higher interval percentage correlates to higher sorting.
	+3.5 to −4	
	−4 to −11	Lower interval percentage correlates to higher sorting.
	−11 to −18	

Figure 12 summarizes the order of single parameters of air velocity and wind pressure in seven distribution modes. Considering the windward air velocity, the layout of uniform building height (UBH), east side high (1-E) and west and north side high (2-WN) is more suitable. Considering the leeward air velocity, the layout of north side high (1-N), east and north side high (2-EN) and east side high (1-E) had an improved ventilation effect, which would be conducive to the diffusion of pollutants.

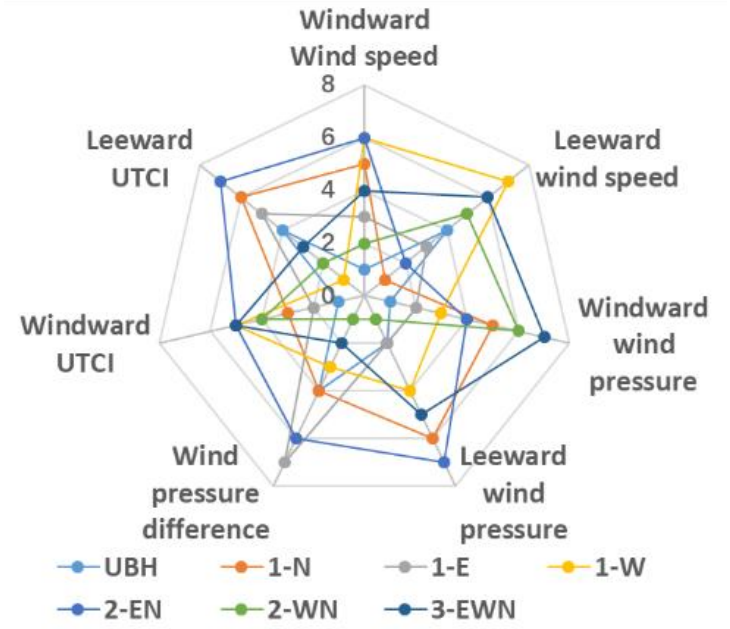

Figure 12. Wind environment and UTCI parameter ranking under seven distribution modes.

With respect to the windward wind pressure statistics, the uniform building height (UBH), the east side high (1-E), and the west side high (1-W) demonstrated the ideal wind pressure effect and were beneficial to indoor natural ventilation on the one side. Based on leeward wind pressure results, the ideal unilateral wind pressure could be obtained at the west and north side high (2-WN), uniform building height (UBH), and the east side height (1-E). With respect to the wind pressure difference results, the west and north side high (2-WN), east–west height (1-W), north side high (1-N), and the west side height (1-W) were more conducive to natural ventilation of the building.

Evaluation ranking of the UTCI-based comfort indicated that there were more comfort spaces on the windward side in the uniform building height (UBH), east side high (E-1), and north side high (N-1). Considering the leeward results, in the layout of the west side high (W-1), west and north side high (2-WN), east–west side high (3-EWN) and north side high (1-N), the comfortable space is higher.

The ranking of air velocity and wind pressure for each building layout was summated to obtain the rationality order of the wind environment, namely: building height (UBH) > east side high (1-E) > uniform west and north side high (2-WN) > north side high (1-N) > west side high (1-W) > east–west and north side high (3-EWN) > east and north side high (2-EN).

4. Discussion

The effect of wind velocity in a high-rise residential area in Harbin was investigated by observing baseline situation data of the typical building height to identify distribution patterns, on which abstract modeling was performed. The accuracy of the CFD simulation settings and output results were verified via wind tunnel tests and the wind speed, wind pressure, UTCI, and other data under different height distribution modes were calculated to explore the relationship between these data and building height spatial layouts. This will assist in providing a spatial layout reference for the future construction of high-rise residential areas in Harbin, which will improve the comfort of living space.

This study analyzed a 3D layout model of high-rise residential buildings in Harbin relative to the wind environment and thermal comfort changes to determine the most suitable building spatial layout. However, this study did not perform correlation analysis between multi-story residential space, i.e., height less than 30 m [19], and other land use space [38]. In the future, additional 3D models could be added to analyze the wind

environment and comfort state in other land use spaces, so that the research would have wider applicability.

With the assistance of wind tunnel tests, the vertical CFD simulation, based on the Phoenics model, of high-rise buildings can improve the accuracy of experimental results relating to grid scale, turbulence models, and iterative processes and can also analyze the vertical effect on high-rise buildings. The wind environment for each spatial layout could also be clarified. However, the selected meteorological conditions for research were too simple. In the future, more detailed meteorological data, such as winter and summer variation [54,55], or monthly variation [56], is needed to obtain more detailed information on the vertical wind environment.

In this study, UTCI was used to study thermal comfort levels resulting from the vertical wind environment in high-rise residential areas in Harbin. Compared with previous studies [50,52], UTCI was incorporated and the relationship between thermal comfort of space and the vertical wind environment was evaluated. The current limitation is that UTCI adaptation to the change in regional climate still needs to be explored further to identify the potential requirements in other cities in cold regions.

5. Conclusions

With respect to high-rise residential buildings, the wind environment at different heights is equally important for people's comfort levels. Therefore, study of the vertical wind environment distribution at high-rise residential buildings based on a suitable layout will be beneficial to the improvement of the comfort levels in residential spaces. Assessing the high-rise residential areas in Harbin as the study subject, the wind environment conditions and the distribution of wind velocity, wind pressure, and UTCI on the building surface have been studied by considering different height modes to improve spatial comfort and to inform suitable building layout. The study reached the following conclusions:

(1) Seven typical height distribution patterns relating to the current high-rise residential communities in Harbin were statistically determined, and included: UBH, 1-N, 1-E, 1-W, 2-EN, 2-WN, and 3-EWN. The results can be used as a reference model for similar simulation and urban planning schemes in the future.

(2) The CFD simulation of the wind environment can be verified by wind tunnel testing to improve the rationality of the simulation settings and the accuracy of the simulation results. Wind environmental indicators, including air velocity and wind pressure, are distributed along the vertical plane of buildings and the trend changes with height. Buildings in the upwind direction are strongly consistent, while buildings in the downwind direction have weak regularity in their changing trend.

(3) The sorting results from seven typical height distribution patterns demonstrated that the contour height parallel to row spacing is the most conducive to the creation of comfortable wind environment space, however, this option is restricted by the plot ratio or site conditions. The northwest height layout pattern is also conducive to the improvement of the vertical wind environment. The selected layout in the case of tall single-row buildings should be on the east or north side. The layout of buildings with high east, west and north sides, and east–north side height, is not conducive to spatial comfort, which should be avoided in future development planning.

(4) In the UTCI comfort evaluation of seven typical height distribution modes, the comfort zone on the windward side reaches 79%, and on the leeward side exceeds 92%. The different distribution locations of high-rise buildings have an impact on the comfort level in different buildings, and the same requirements regarding layout and wind environment should be applied.

Considering future urban development, it is necessary to formulate corresponding norms and standards, clarify the position of high-rise buildings in the landscape, and ensure correct building spacing. To obtain adequate ventilation and comfort, the installation of inward-opening windows, which push away from the bottom, and reinforcement and blocking of roof windows to block air flow, should be considered for buildings located in areas that may result in discomfort.

Author Contributions: Conceptualization, D.S. (Di Song); Data curation, D.S. (Di Song), D.S. (Da Shi) and L.W.; Formal analysis, D.S. (Di Song); Funding acquisition, J.L. and M.L.; Investigation, D.S. (Di Song) and D.S. (Da Shi); Methodology, D.S. (Di Song) and D.S. (Da Shi); Project ad-ministration, J.L. and M.L.; Resources, J.L. and M.L.; Software, D.S. (Di Song) and L.W.; Supervision, J.L. and M.L.; Validation, D.S. (Di Song) and L.W.; Visualization, D.S. (Di Song) and D.S. (Da Shi); Writing—original draft, D.S. (Di Song); Writing—review and editing, D.S. (Di Song), M.L. and D.S. (Da Shi). All authors have read and agreed to the published version of the manuscript.

Funding: This research was funded by National Natural Science Foundation of China, grant number 51878208.

Conflicts of Interest: The authors declare no conflict of interest. The funder had no role in the design of the study; in the collection, analyses, or interpretation of data; in the writing of the manuscript, or in the decision to publish the results.

Appendix A

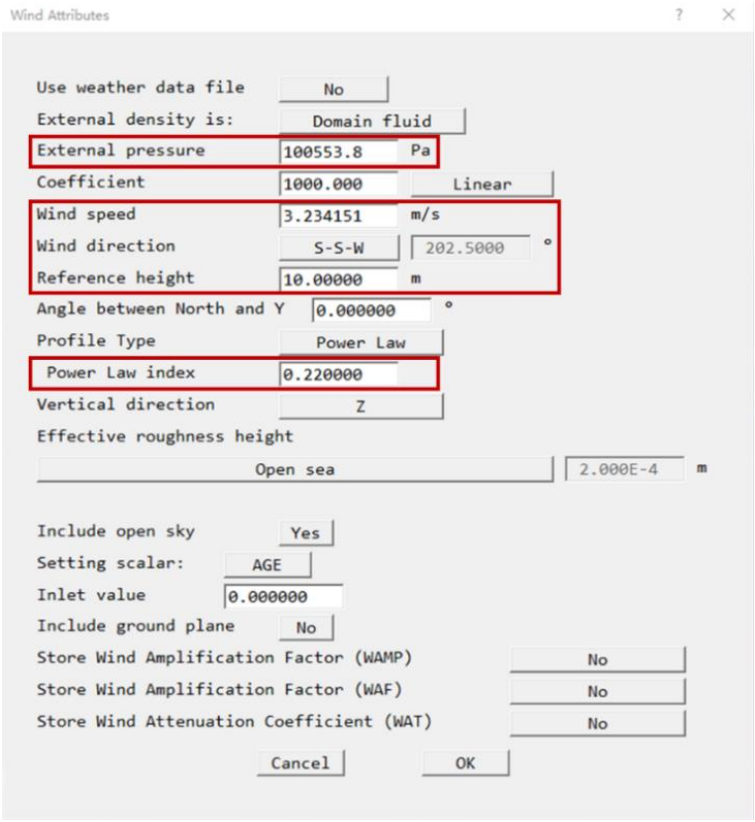

Figure A1. Phoenics wind environment attribute interface.

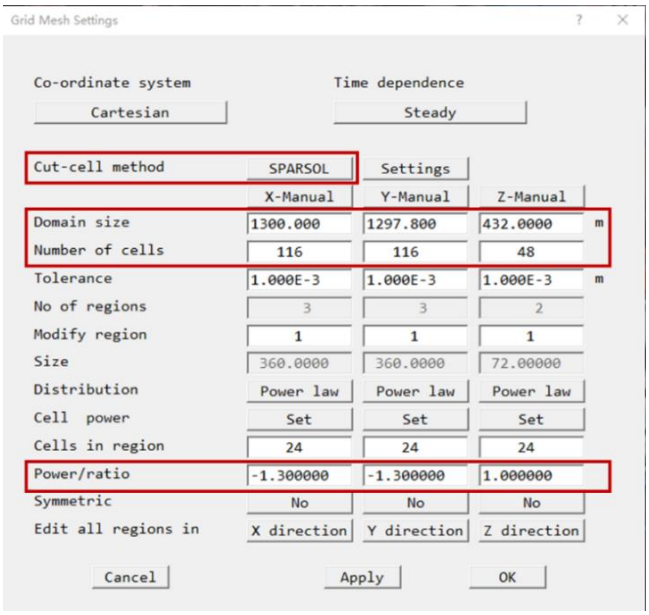

Figure A2. Phoenics grid mesh settings interface.

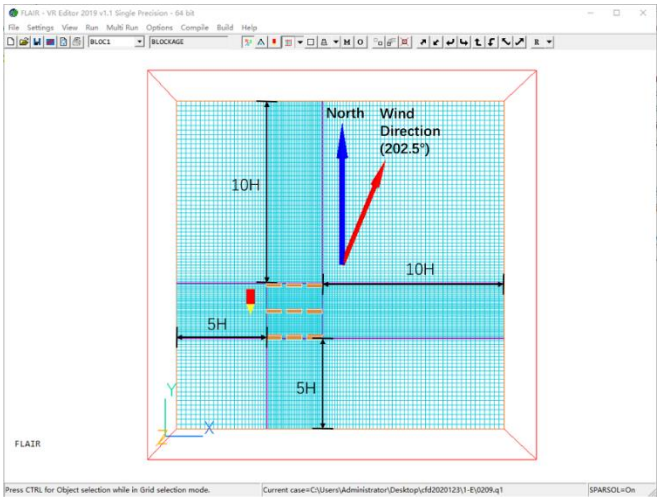

Figure A3. The XY plane grid distribution for seven layout modes (1-E used as the example).

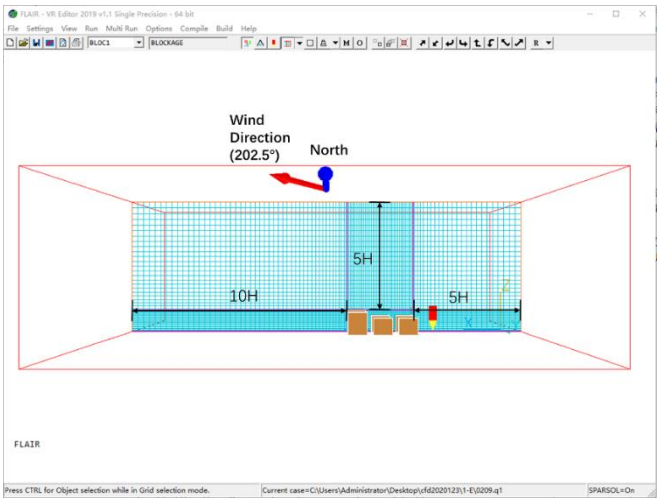

Figure A4. The Z plane grid distribution for seven layout modes (1-E used as the example).

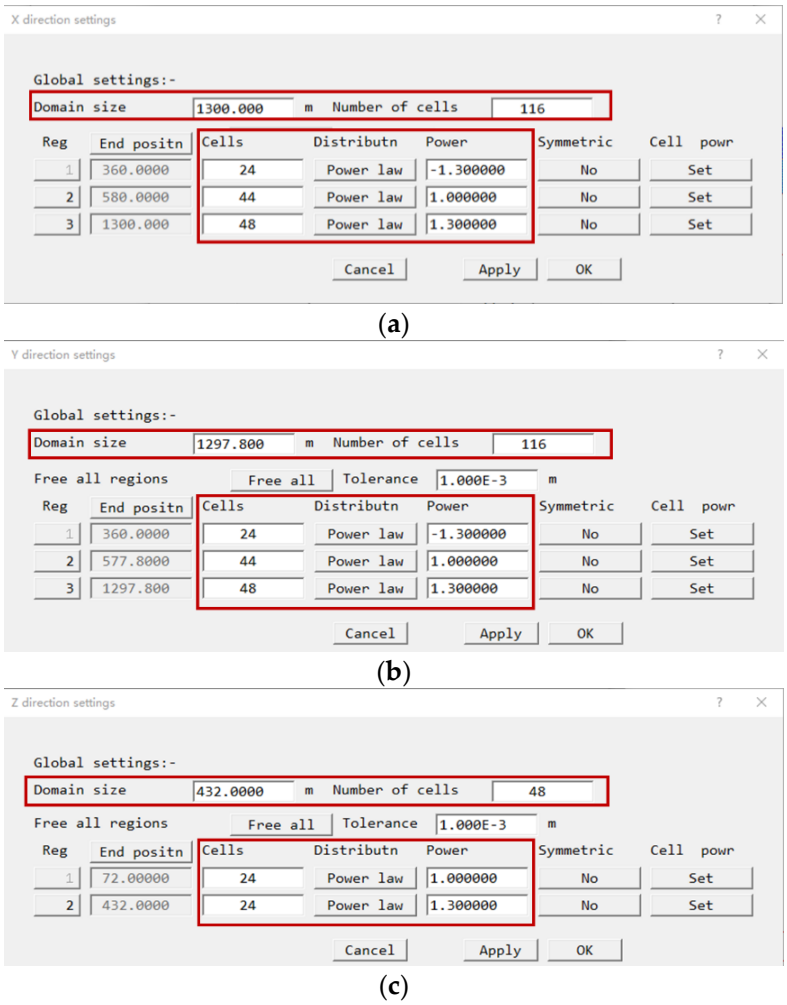

Figure A5. The XYZ direction grid settings (**a**) X axis, (**b**) Y axis, and (**c**) Z axis.

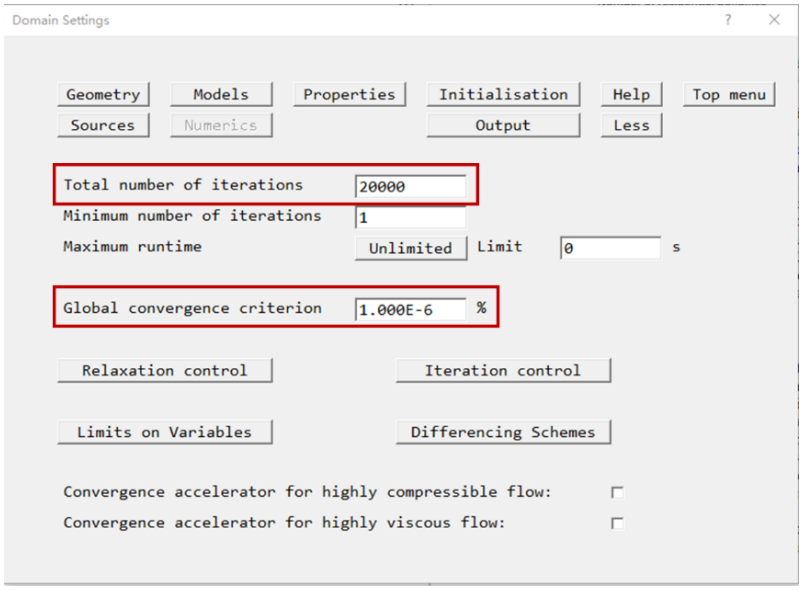

Figure A6. Iteration steps and residual settings.

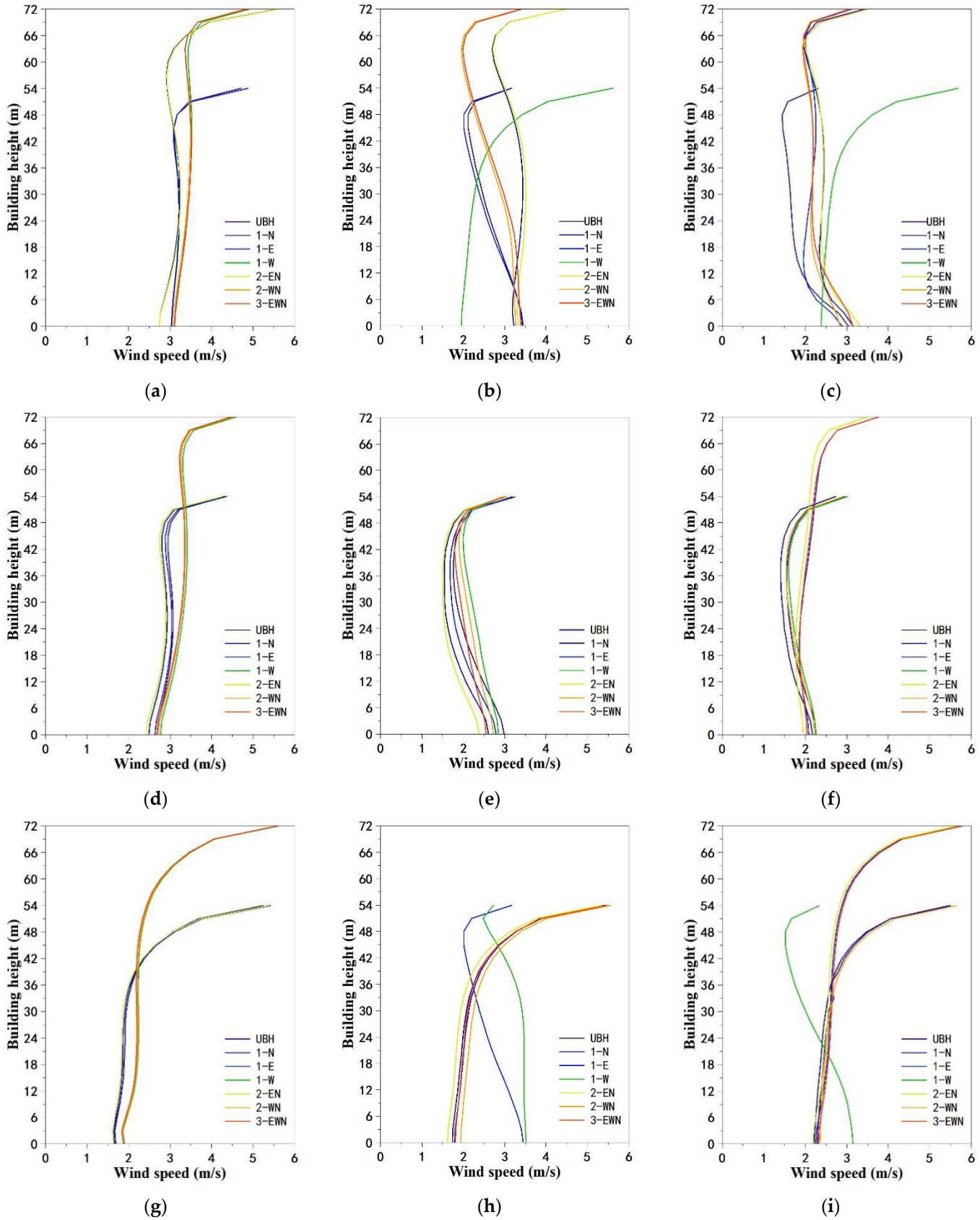

Figure A7. Air velocity on the windward side of single buildings under seven operating conditions; (**a**) building #1, (**b**) building #2, (**c**) building #3, (**d**) building #4, (**e**) building #5, (**f**) building #6, (**g**) building #7, (**h**) building #8, and (**i**) building #9.

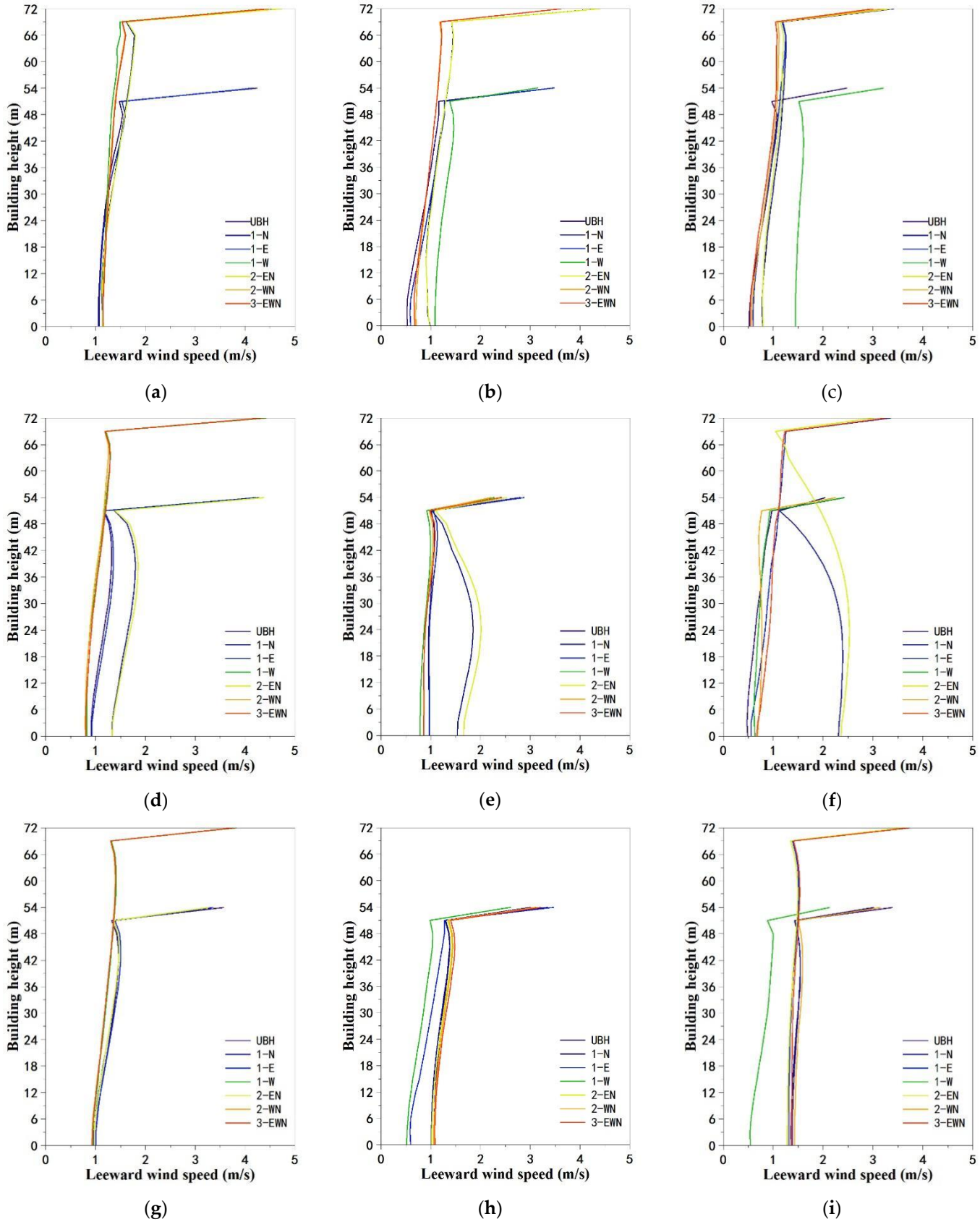

Figure A8. Air velocity on the leeward side of single buildings under seven operating conditions; (**a**) building #1, (**b**) building #2, (**c**) building #3, (**d**) building #4, (**e**) building #5, (**f**) building #6, (**g**) building #7, (**h**) building #8, and (**i**) building #9.

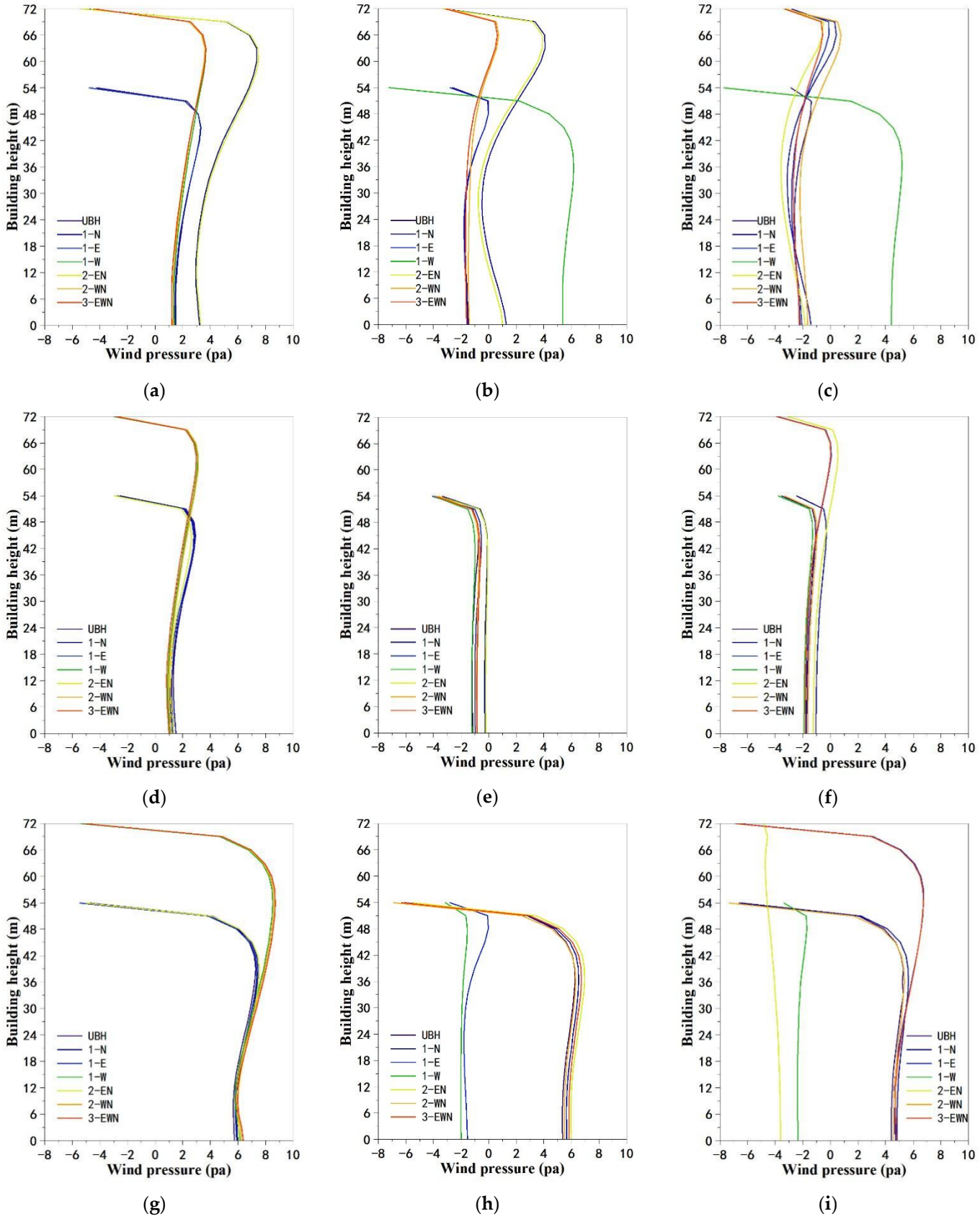

Figure A9. Wind pressure on the windward side of single buildings under seven operating conditions; (**a**) building #1, (**b**) building #2, (**c**) building #3, (**d**) building #4, (**e**) building #5, (**f**) building #6, (**g**) building #7, (**h**) building #8, and (**i**) building #9.

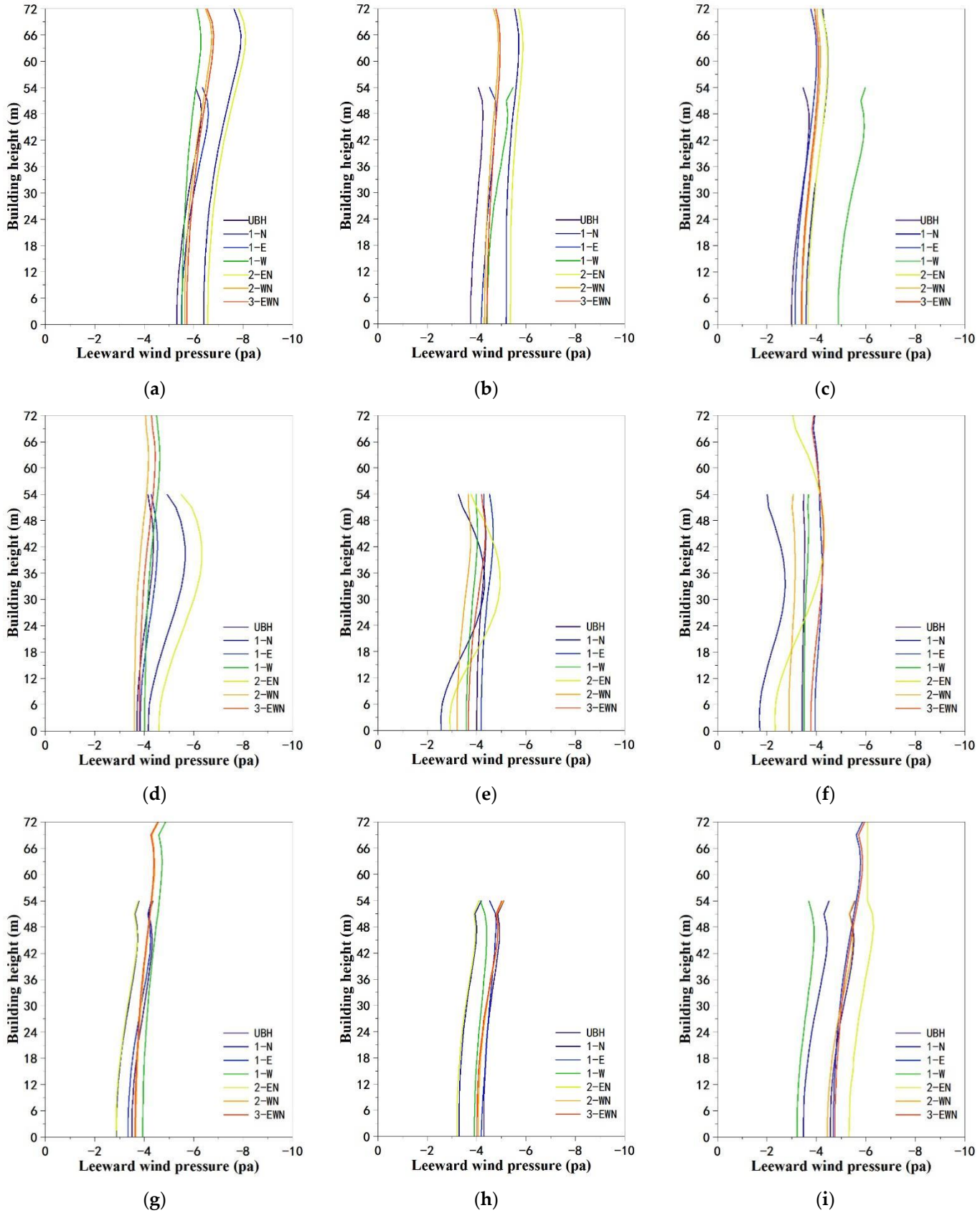

Figure A10. Wind pressure on the leeward side of single buildings under seven operating conditions; (**a**) building #1, (**b**) building #2, (**c**) building #3, (**d**) building #4, (**e**) building #5, (**f**) building #6, (**g**) building #7, (**h**) building #8, and (**i**) building #9.

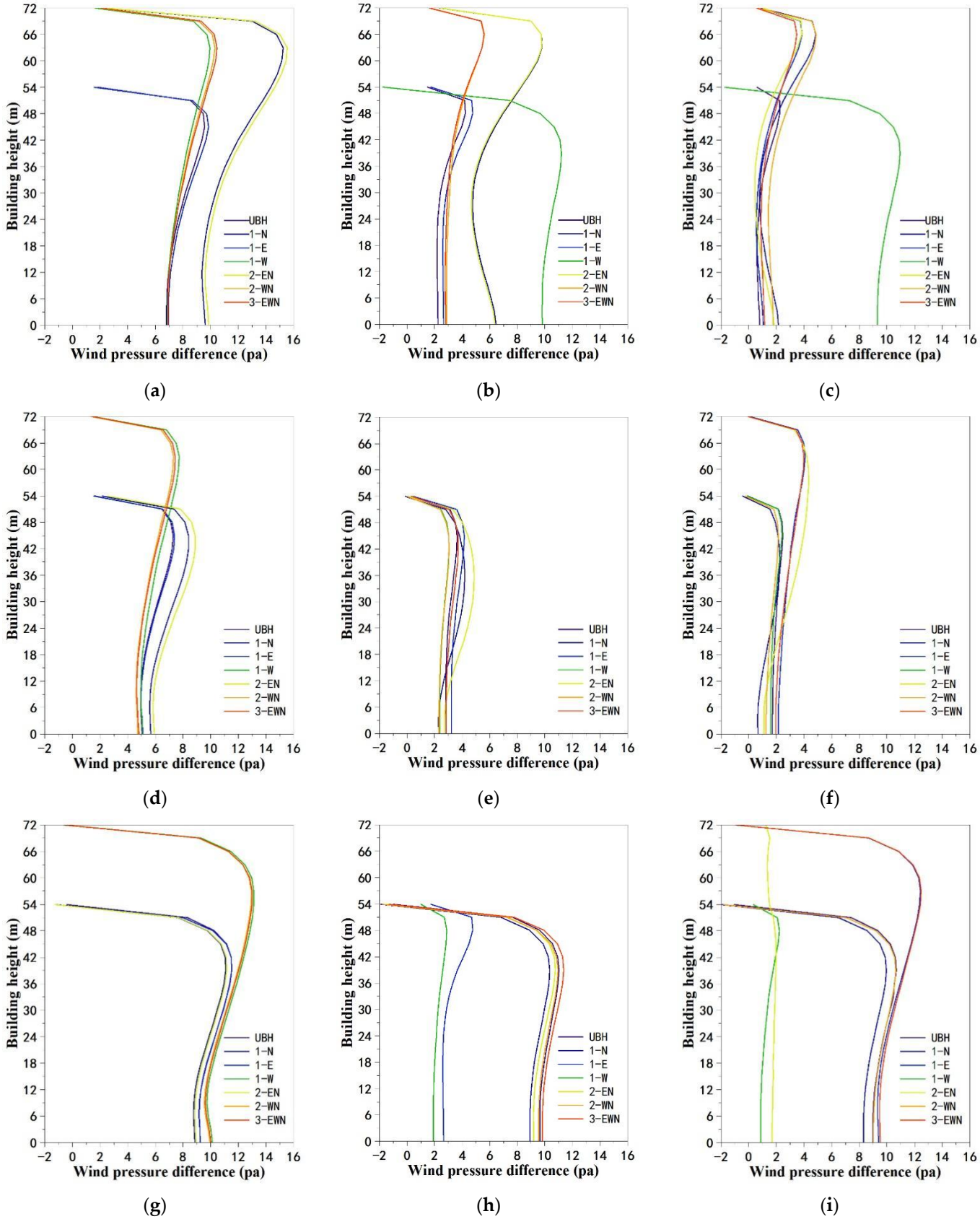

Figure A11. Wind pressure difference of individual buildings under seven operating conditions; (**a**) building #1, (**b**) building #2, (**c**) building #3, (**d**) building #4, (**e**) building #5, (**f**) building #6, (**g**) building #7, (**h**) building #8, and (**i**) building #9.

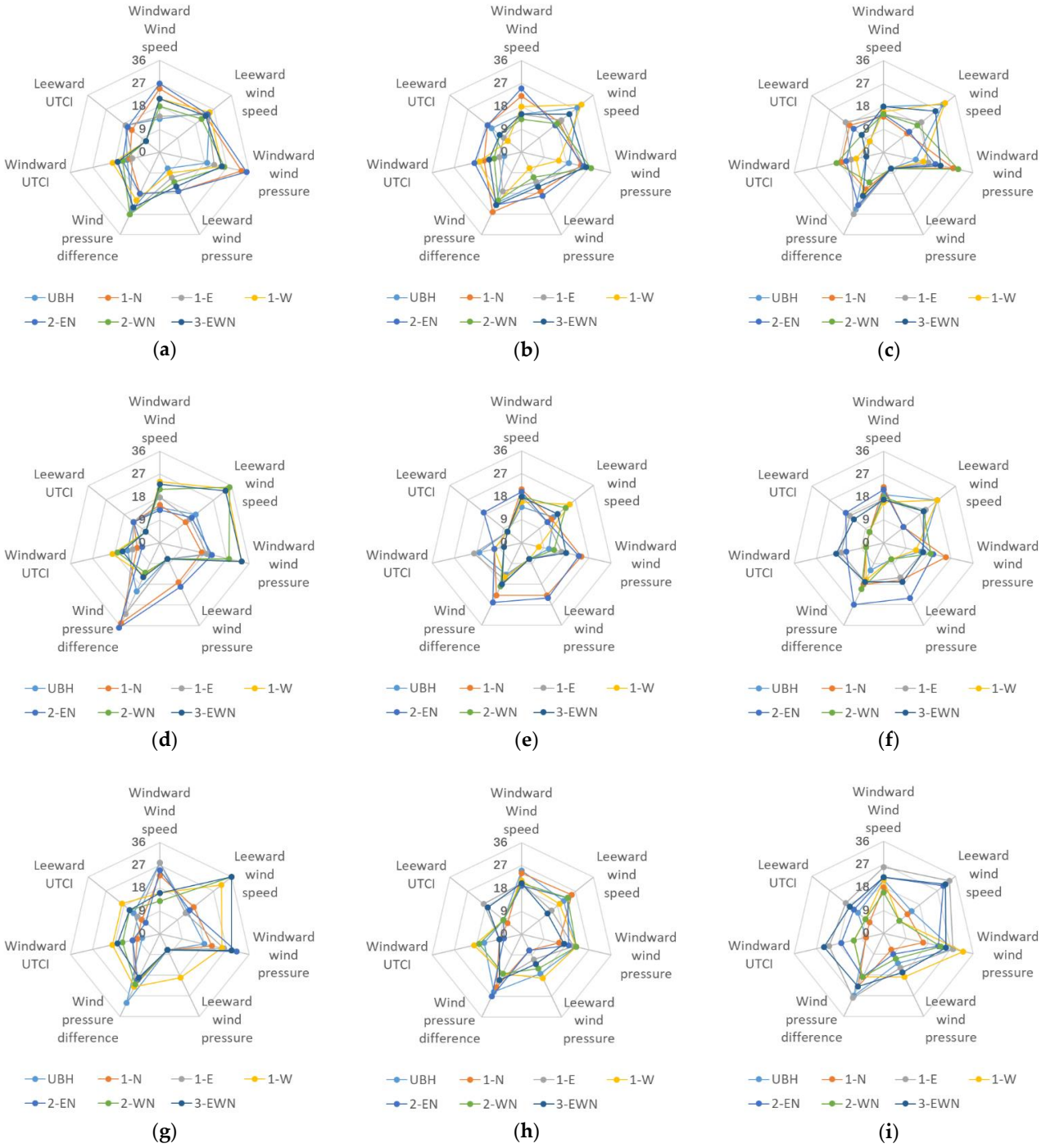

Figure A12. Results summary of single building wind environment parameters and UTCI under seven layouts; (**a**) building #1, (**b**) building #2, (**c**) building #3, (**d**) building #4, (**e**) building #5, (**f**) building #6, (**g**) building #7, (**h**) building #8, and (**i**) building #9.

References

1. Zhang, D.; Xu, J.; Zhang, Y.; Wang, J.; He, S.; Zhou, X. Study on sustainable urbanization literature based on Web of Science, scopus, and China national knowledge infrastructure: A scientometric analysis in CiteSpace. *J. Clean Prod.* **2020**, *264*, 121537. [CrossRef]
2. Juan, Y.H.; Wen, C.Y.; Li, Z.; Yang, A.S. Impacts of urban morphology on improving urban wind energy potential for generic high-rise building arrays. *Appl. Energy* **2021**, *299*, 117304. [CrossRef]
3. He, Q.H.; Ossain, M.; Ng, S.T.; Augenbroe, G.L. Retrofitting high-rise residential building in cold and severe cold zones of China—A deterministic decision-making mechanism. *Sustainability* **2020**, *12*, 5831. [CrossRef]

4. Lei, Y.; Yong, Y.Y.; Zhang, L. Influence of waterside buildings' layout on wind environment and the relation with design based on a case study of the she kou residential district. *J. Archit. Environ. Struct. Eng. Res.* **2021**, *4*, 20–30.
5. Yang, F.; Chen, L. *Pedestrian Wind in High-Rise Residential Quarters, High-Rise Urban Form and Microclimate*; Springer: Singapore, 2020; pp. 111–137.
6. Cammelli, S.; Stanfield, R. Meeting the challenges of planning policy for wind microclimate of high-rise developments in London. *Procedia Eng.* **2017**, *198*, 43–51. [CrossRef]
7. Aristodemou, E.; Boganegra, L.M.; Mottet, L.; Pavlidis, D.; Constantinou, A.; Pain, C.; Robins, A.; ApSimon, H. How tall buildings affect turbulent air flows and dispersion of pollution within a neighbourhood. *Environ. Pollut.* **2018**, *233*, 782–796. [CrossRef]
8. Lin, G.; Zhang, S.; Zhong, Y.; Zhang, L.; Ai, S.; Li, K.; Su, W.; Cao, L.; Zhao, Y.; Tian, F.; et al. Community evidence of severe acute respiratory syndrome coronavirus 2 (SARS-CoV-2) transmission through air. *Atmos. Environ.* **2021**, *246*, 118083. [CrossRef]
9. Coccia, M. How (un)sustainable environments are related to the diffusion of COVID-19: The relation between coronavirus Disease 2019, air pollution, wind resource and energy. *Sustainability* **2020**, *12*, 9709. [CrossRef]
10. Liu, Z.; Zhao, X.; Jin, Y.; Jin, H.; Xu, X. Prediction of outdoor human thermal sensation at the pedestrian level in high-rise residential areas in severe cold regions of China. *Energy Procedia* **2019**, *157*, 51–58. [CrossRef]
11. Zhang, J.; Zhang, X. Pedestrian-level wind environment assessment of Shenyang's residential areas through numerical simulations. *Sustainability* **2021**, *14*, 380. [CrossRef]
12. Xia, D.; Wang, J.; Sun, L.Y.; Tu, J.W.; Sun, X. Numerical simulation of wind environment and outdoor comfort surrounding a typical super high-rise building cluster in Zhuhai. *Acta Sci. Nat. Univ. Sunyatseni* **2019**, *58*, 42–52.
13. Florea, I.B.; Iagar, O.A.; Vladut, C.A.; Cosoiu, C.I.; Degeratu, M. Wind tunnel modelling of a residential ensemble in a high rise building urban area. *IOP Conf. Ser. Earth Environ. Sci.* **2021**, *664*, 012023. [CrossRef]
14. Yt, A.; Msa, B. Wind tunnel measurement of three-dimensional turbulent flow structures around a building group: Impact of high-rise buildings on pedestrian wind environment. *Build. Environ.* **2021**, *206*, 108389.
15. Li, M.; Qiu, X.; Shen, J.; Xu, J.; Feng, B.; He, Y.; Shi, G.; Zhu, X. CFD simulation of the wind field in Jinjiang City using a building data generalization method. *Atmosphere* **2019**, *10*, 326. [CrossRef]
16. El-Heweity, M.M.; Abdelnaby, M.H.; Eshra, E.M. Numerical simulation of buffeting longitudinal wind forces on buildings. *Alex. Eng. J.* **2019**, *58*, 225–236. [CrossRef]
17. Limona, S.S.; Al-Hagla, K.S.; El-Sayad, Z.T. Using simulation methods to investigate the impact of urban form on human comfort. Case study: Coast of Baltim, North Coast, Egypt. *Alex. Eng. J.* **2019**, *58*, 273–282. [CrossRef]
18. Toparlar, Y.; Blocken, B.; Maiheu, B.; van Heijst, G. A review on the CFD analysis of urban microclimate. *Renew. Sust. Energ. Rev.* **2017**, *80*, 1613–1640. [CrossRef]
19. Jin, H.; Liu, Z.; Jin, Y.; Kang, J.; Liu, J. The effects of residential area building layout on outdoor wind environment at the pedestrian level in severe cold regions of China. *Sustainability* **2017**, *9*, 2310. [CrossRef]
20. Li, B.; Li, X.-B.; Li, C.; Zhu, Y.; Peng, Z.-R.; Wang, Z.; Lu, S.-J. Impacts of wind fields on the distribution patterns of traffic emitted particles in urban residential areas. *Transport. Res. Part D-Transport. Environ.* **2019**, *68*, 122–136. [CrossRef]
21. Antoniou, N.; Montazeri, H.; Neophytou, M.; Blocken, B. CFD simulation of urban microclimate: Validation using high-resolution field measurements. *Sci. Total Environ.* **2019**, *695*, 133743. [CrossRef]
22. Zeng, S.; Tian, J.; Zeng, J. A study on ventilation efficiency and optimal layout of typical residential modules based on CFD simulation. *Archit. J.* **2019**, *2*, 24–30.
23. Wang, W.; Deng, Z.J.; Hu, C. Comparison and evaluation of wind environment simulation of mixed settlements in hefei. *Ind. Constr.* **2018**, *48*, 54–59.
24. Huang, W.F.; Zhou, T.; Chen, X. Wind environment assessment of typical building groups by using CFD numerical simulation. *J. Hefei Univ. Technol.* **2019**, *42*, 415–421.
25. *GB50352-2019*; China Institute of Building Standard Design & Research. Uniform Standard for Design of Civil Buildings. China Architecture & Building Press: Beijing, China, 2019; pp. 1–68.
26. *GB50016-2014*; China Institute of Building Standard Design & Research. Architectural Design Code for Fire Protection. China Planning Press: Beijing, China, 2015; pp. 1–74.
27. *GB50096-2011*; China Architecture Design & Research Group. Design Code for Residential Buildings. China Architecture & Building Press: Beijing, China, 2012; pp. 1–98.
28. *GB50180-2018*; China Academy of Urban Planning & Design. Standard for Urban Residential Area Planning and Design. China Architecture & Building Press: Beijing, China, 2018; pp. 1–43.
29. Several Opinions of the Harbin Municipal People's Government on the Implementation of the "Harbin Urban and Rural Planning Regulations". Available online: http://www.harbin.gov.cn/art/2012/8/8/art_226_3039.html (accessed on 8 April 2022).
30. Li, X.; Wang, J.; Eftekhari, M.; Qi, Q.; Jiang, D.; Song, Y.; Tian, P. Improvement strategies study for outdoor wind environment in a university in Beijing based on CFD simulation. *Adv. Civ. Eng.* **2020**, *2020*, 1–14. [CrossRef]
31. The National Climatic Data Center (NCDC) Public FTP Server. Available online: ftp://ftp.ncdc.noaa.gov/pub/data/noaa/isd-lite/ (accessed on 4 April 2022).
32. Yang, M.C.; Li, Y.W. Simulation analysis of winter monsoon environment and spatial strategy research in large-scale residential area—A case study of Nanhu large-scale residential area in Wuhan City. In Vibrant Urban and Rural Areas and Beautiful Human Settlements—Proceedings of the 2019 China Urban Planning Annual Meeting (05 Application of New Technologies in Urban

Planning). China Urban Planning Society, Chongqing Municipal People's Government, Chongqing, China,, 19–21 October 2019; Urban Planning Society of China: Beijing, China, 2019.
33. *JGJ286-2013*; South China University of Technology. Design Standard for Thermal Environment of Urban Residential Areas. China Architecture & Building Press: Beijing, China, 2014; pp. 1–78.
34. Liu, S.; Pan, W.; Zhao, X.; Zhang, H.; Cheng, X.; Long, Z.; Chen, Q. Influence of surrounding buildings on wind flow around a building predicted by CFD simulations. *Build. Environ.* **2018**, *140*, 1–10. [CrossRef]
35. Baetke, F.; Werner, H.; Wengle, H. Numerical simulation of turbulent flow over surface-mounted obstacles with sharp edges and corners. *J. Wind Eng. Ind. Aerodyn.* **1990**, *35*, 129–147. [CrossRef]
36. Zhuang, Z.; Yu, Y.; Ye, H.; Tan, H.; Xie, J. Review on CFD Simulation Technology of Wind Environment around Buildings. *Build. Sci.* **2014**, *30*, 108–114.
37. Guo, F.; Zhu, P.; Wang, S.; Duan, D.; Jin, Y. Improving natural ventilation performance in a high-density urban district: A building morphology method. *Procedia Eng.* **2017**, *205*, 952–958. [CrossRef]
38. Ying, X.; Wang, Y.; Li, W.; Liu, Z.; Ding, G. Group layout pattern and outdoor wind environment of enclosed office buildings in Hangzhou. *Energies* **2020**, *13*, 406. [CrossRef]
39. Franke, J.; Hellsten, A.; Schlünzen, H.; Carissimo, B. Best practice guideline for the CFD simulation of flows in the urban environment. In *COST Action 732, Quality Assurance and Improvement of Microscale Meteorological Models*; COST Office: Brussels, Belgium, 2007; pp. 1–53.
40. Jiang, Z.; Gao, W. Impact of enclosure boundary patterns and lift-up design on optimization of summer pedestrian wind environment in high-density residential districts. *Energies* **2021**, *14*, 3199. [CrossRef]
41. *JGJ/T338-2014*; China Academy of Building Research. Standard for Wind Tunnel Test of Buildings and Structures. China Architecture & Building Press: Beijing, China, 2015; pp. 1–71.
42. *JTG/T3360-01-2018*; Tongji University. Wind-Resistent Design Specification for Highway Bridges. China Communications Press: Beijing, China, 2019; pp. 157–186.
43. Terjung, W.H. Physiologic climates of the conterminous united states: A bioclimatic classification based on man. *Ann. Assoc. Am. Geogr.* **2015**, *56*, 141–179. [CrossRef]
44. *JGJ286-2013*; China Academy of Building Research; Shanghai Research Institute of Building Sciences (Group) Co, Ltd. Assessment Standard for Green Building. China Architecture & Building Press: Beijing, China, 2019; pp. 1–35.
45. Tan, L.W. Simulation of Outdoor Wind Environment in Residential Area Based on Reasonable Static Wind Rate. Master's Thesis, Chongqing University, Chongqing, China, 2017.
46. Xi, R. Study on Residential Area Layout Based on Reasonable Silent Area a Case Study of Residential District in Xi'an. Master's Thesis, Chongqing University, Chongqing, China, 2017.
47. *DB23/T 1642-2020*; Heilongjiang Province Academy of Cold Area Building Research. Assessment Standard for Green Building of Heilongjiang Province. Harbin Institute of Technology Press: Harbin, China, 2020; pp. 1–113.
48. Nie, H.S.; Qin, Y.G. *Chinese Ecological Residential Assessment Manual*; China Architecture & Building Press: Beijing, China, 2002; pp. 1–52.
49. Silva, T.J.V.; Hirashima, S.Q.S. Predicting urban thermal comfort from calibrated UTCI assessment scale—A case study in Belo Horizonte city, southeastern Brazil. *Urban Clim.* **2020**, *36*, 100652. [CrossRef]
50. Zhu, Z. Research on the Form Design of Commercial District Building Group in The Severe Cold Region Based on Outdoor Thermal Comfort. Master's Thesis, Harbin Institute of Technology, Harbin, China, 2020.
51. Zhu, N.; Wang, C.; Zhou, H.Z.; Li, M. Spatial pattern analysis of instantaneous thermal field in Harbin. *Chin. J. Appl. Ecol.* **2003**, *11*, 1955–1958.
52. Zhi, D.Y. Research on Design Strategy of University'S Teaching Buildings Based on Outdoor Thermal Comfort. Master's Thesis, Harbin Institute of Technology, Harbin, China, 2019.
53. UTCI—Universal Thermal Climate Index. Available online: http://www.utci.org/index.php (accessed on 13 April 2022).
54. Jiang, X.B.; Yang, C.Z.; Tang, B.; Chen, W. Coupled simulation and analysis of wind environment around residential quarter in hot summer and cold winter area in China. *Adv. Mater. Res.* **2013**, *726–731*, 3627–3632. [CrossRef]
55. Du, Y.; Mak, C.M.; Kwok, K.; Tse, K.T.; Lee, T.C.; Ai, Z.T.; Liu, J.L.; Niu, J.L. New criteria for assessing low wind environment at pedestrian level in Hong Kong. *Build. Environ.* **2017**, *123*, 23–36. [CrossRef]
56. Kubota, T.; Miura, M.; Tominaga, Y.; Mochida, A. Wind tunnel tests on the relationship between building density and pedestrian level wind velocity: Development of guidelines for realizing acceptable wind environment in residential neighborhoods. *Build. Environ.* **2008**, *43*, 1699–1708. [CrossRef]